Supporting Information

Concentrated Electrolytes: Decrypting Electrolyte Properties and Reassessing Al Corrosion Mechanisms

Dennis W. McOwen,[a] Daniel M. Seo,[a] Oleg Borodin,[b] Jenel Vatamanu,[c] Paul D. Boyle[d] and Wesley A. Henderson*[a]

[a]Ionic Liquids & Electrolytes for Energy Technologies (ILEET) Laboratory
Department of Chemical & Biomolecular Engineering
North Carolina State University
911 Partners Way, Raleigh, North Carolina 27695, USA
E-mail: whender@ncsu.edu

[b]Electrochemistry Branch, Sensor & Electron Devices Directorate
U.S. Army Research Laboratory
Adelphi, Maryland 20783, USA

[c]Deparment of Material Science and Engineering
University of Utah
Salt Lake City, Utah 84112, USA

[d]X-ray Structural Facility
Department of Chemistry
North Carolina State University
2620 Yarbrough Drive, Raleigh, North Carolina 27695, USA

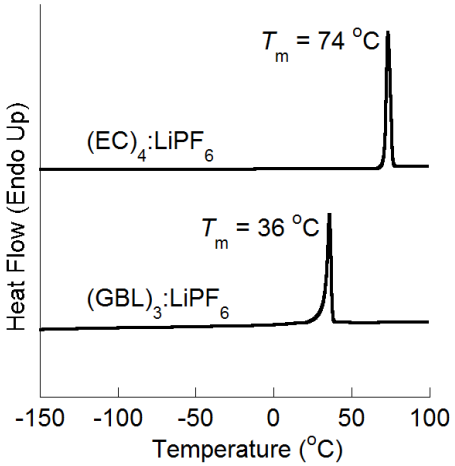

Figure S1. DSC for two high melting crystalline $LiPF_6$ solvates with EC and γ-butyrolactone (GBL): $(EC)_4$:$LiPF_6$ and $(GBL)_4$:$LiPF_6$.

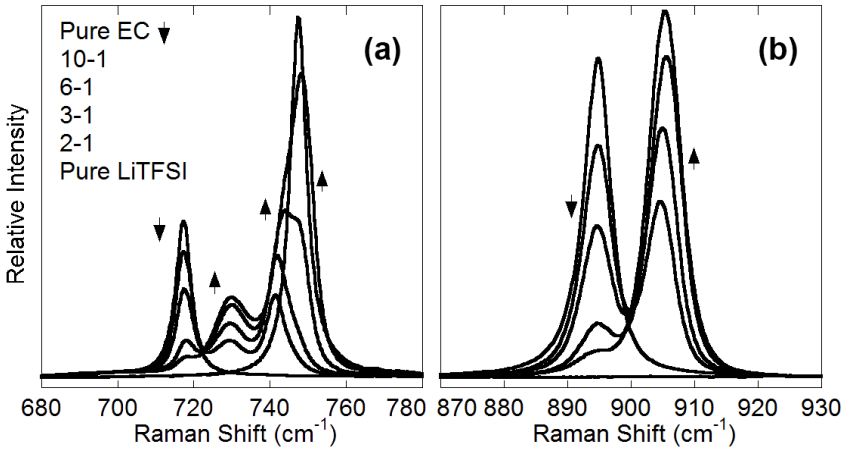

Figure S2. Raman spectra of EC ring breathing modes at (a) 717 cm^{-1} and (b) 895 cm^{-1} for the EC-LiTFSI electrolytes (EC-Li ratio indicated). Peaks above 735 cm^{-1} are due to $TFSI^-$ vibrational modes (data for both regions normalized to the EC solvent band: 850-950 cm^{-1}).

Raman Scattering Activity Correction Factors (i.e., Scaling Factors):

As noted in the manuscript (Sections 2 and 3.2), the Raman scattering activities of the two EC vibrational modes that were studied (717 and 895 cm^{-1}) change when the EC molecule is coordinated to a Li^+ cation—that is, the observed intensities of the 717 and 895 cm^{-1} bands are not the same as their coordinated counterparts at 729 and 905 cm^{-1}. Thus, if a mixture contained 50% coordinated and 50% uncoordinated EC, the integrated peak areas of the coordinated and uncoordinated bands would not be equal. QC calculations from the cited previous work (Ref. 27) have been used to obtain the changes in the Raman scattering intensity between the coordinated and uncoordinated EC, thus providing the necessary correction factors. Specifically, a correction factor of 0.88 is applied to the 717 cm^{-1} band and 1.06 to the 905 cm^{-1} band. In addition to the correction factor for the 717 cm^{-1} band, however, a second low intensity EC solvent band located near 695 cm^{-1} (which shifts to 711 cm^{-1} upon Li^+ cation coordination) must also be taken into account for the calculation.

For mixtures of EC with lithium salts that do not have significant anion band overlap with the EC Raman bands, these correction factors have significantly improved the agreement between the calculated fractions of coordinated/uncoordinated EC for the two vibrational modes (Ref. 27). In this work, the same correction factors were used, but the $TFSI^-$ anion band overlap renders deconvolution of the 717 and 729 cm^{-1} bands less accurate (Figures S2 and S3), particularly for high concentrations of LiTFSI ($x > 0.15$). A qualitative agreement between the two regions is still found, however, with the agreement improving for the samples with the highest concentration of LiTFSI. This is likely due to the $TFSI^-$ anion bands shifting to a higher wavenumber, thus making them more readily separable from the 729 cm^{-1} EC solvent band, as the anions become more and more aggregated with increasing LiTFSI concentration (Figures 3 and S2a).

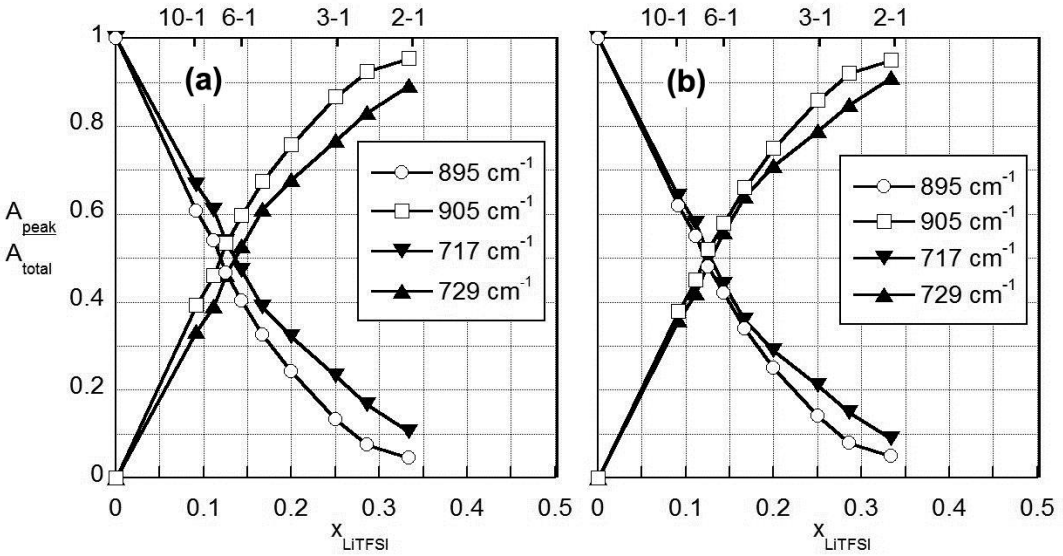

Figure S3. Comparison of the fraction of coordinated and uncoordinated EC in liquid EC-LiTFSI electrolytes at 20 °C determined from the two different EC vibrational modes (two bands each): 895 and 905 cm^{-1} (open circles and squares) and 717 and 729 cm^{-1} (filled triangles). (a) from the fitted raw data and (b) after the correction factors were applied. NOTE: The data obtained from the 717-729 cm^{-1} region of the spectra are expected to be less accurate due to overlap of the solvent bands with the $TFSI^-$ anion bands.

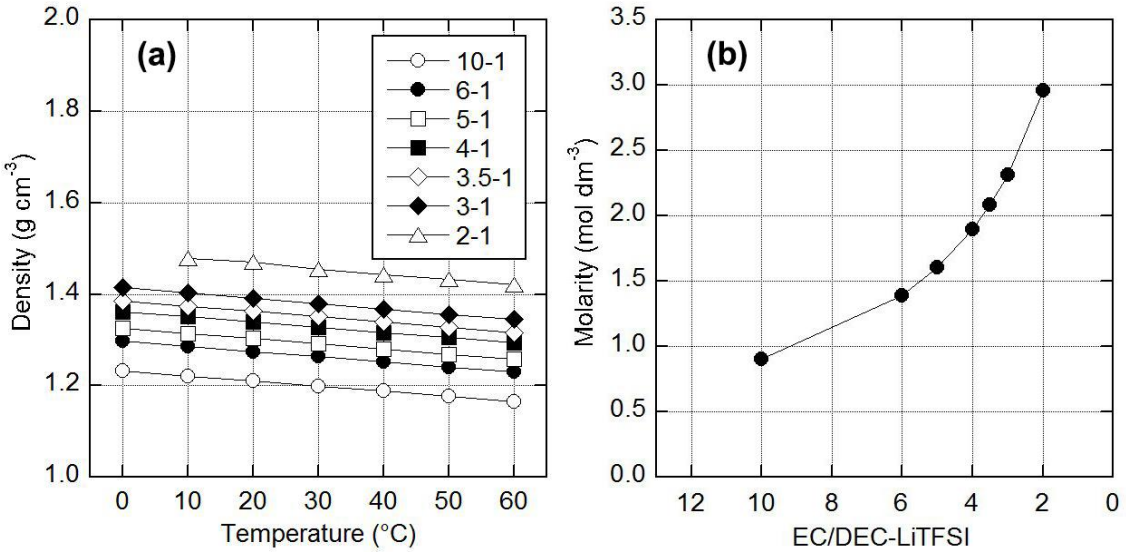

Figure S4. (a) Variable-temperature density of EC/DEC 3/7 (v/v)-LiTFSI electrolytes and (b) the corresponding link between the solvent-LiTFSI molar ratio and electrolyte molarity.

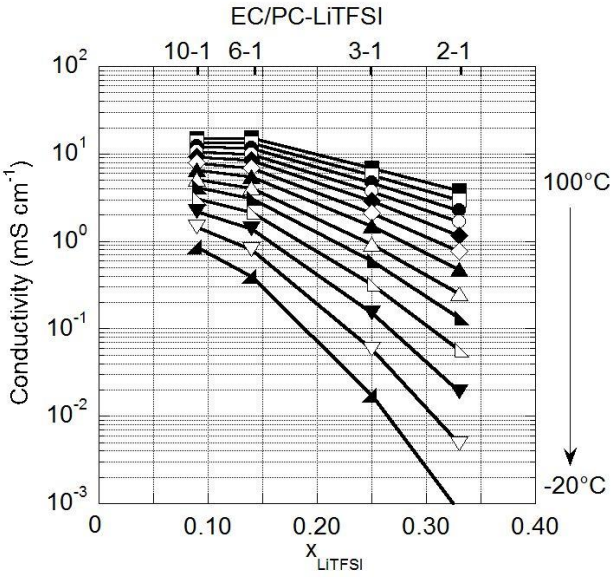

Figure S5. Variable-temperature ionic conductivity of EC/PC 3/7 (v/v)-LiTFSI electrolytes.

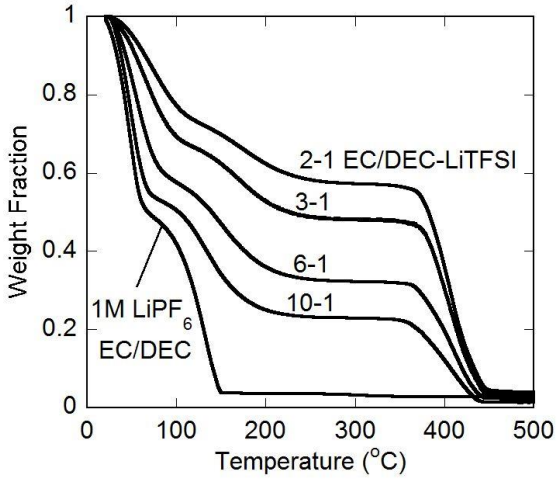

Figure S6. TGA heating traces (5 °C min^{-1}) of 3/7 (v/v) EC/DEC-LiTFSI electrolytes.

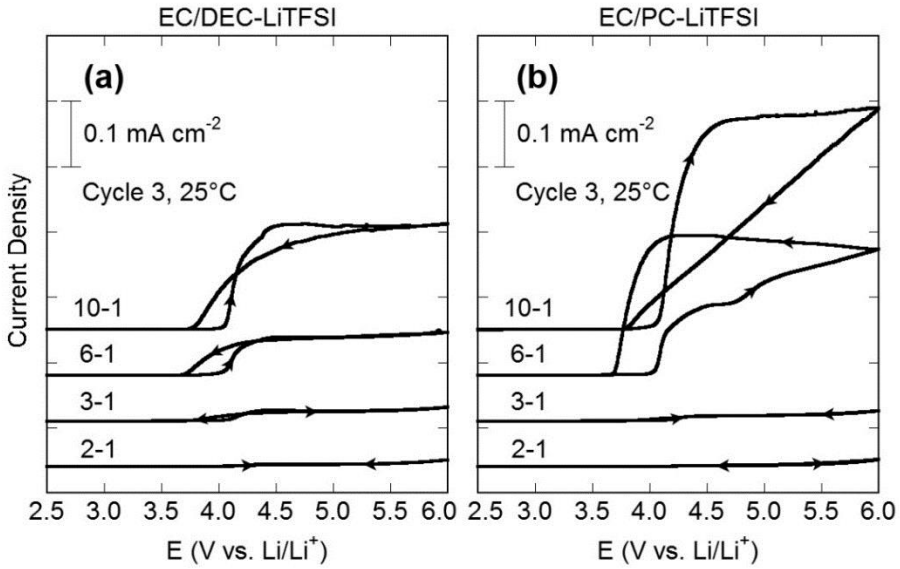

Figure S7. Anodic stability (3rd cycle, 25 °C, 5.0 mV s^{-1}) of coin cells containing (a) EC/DEC 3/7 (v/v)-LiTFSI and (b) EC/PC 3/7 (v/v)-LiTFSI electrolytes using Al foil working electrodes and Li metal counter/reference electrodes.

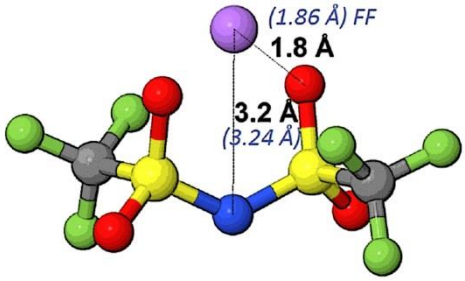

Figure S8. Geometry of the [Li^+-$TFSI^-$] complex from G4MP2 calculations. The G4MP2 distances are shown in black, while distances obtained from molecular mechanics optimization using APPLE&P force field are shown in blue parentheses and italicized.

Molecular Dynamics (MD) Simulations of EC-LiTFSI Electrolytes

Table S1. MD simulations results at 333 K and specification of simulated systems

solvent : Li	20	10	5	2
number of solvent in MD box	640	640	640	384
number salt in MD box	32	64	128	192
concentration (M)	0.66	1.20	2.03	3.48
length of equilibration runs (ns)	3	12	7	10
length of production run (ns)	6.4	9	19	18
ρ (density), MD (kg m^{-3})	1346	1399	1478	1614
ρ (density), experimental (kg m^{-3})	1364	1415	1495	
ρ (density), error %	-1.3	-1.1	-1.1	
Transport Properties				
$D_{solvent}$, MD (10^{-10} m^2 s^{-1})	7.4	5.5	2.8	0.450
D_-, MD (10^{-10} m^2 s^{-1})	4.4	2.7	1.4	0.144
D_+, MD (10^{-10} m^2 s^{-1})	3.5	2.7	1.4	0.166
κ (conductivity), MD (mS cm^{-1})	13.4	11.4	7.8	1.45
κ (conductivity), experimental (mS cm^{-1})	11.5	12.3	8.1	1.3
viscosity, MD (mPa s)	1.9	2.6	5.0	37.3
Ion Coordination				
fraction of free Li^+ (SSIP)	0.62	0.44	0.23	0.05
fraction of free N(TFSI) (SSIP)	0.61	0.38	0.15	0.01
fraction of free EC (not coordinated by Li^+)	0.81	0.66	0.44	0.14
Li^+ coordination numbers				
number O (EC) (r(O-Li) < 2.5 Å)	3.69	3.3	2.78	1.72
number O(TFSI) (r(O-Li) < 2.5 Å)	0.59	0.98	1.52	2.55
number N(TFSI) (r(N-Li) < 4.74 Å)	0.42	0.70	1.10	1.99
fraction of bidentate O(TFSI)/Li^+ coordination*	0.44	0.46	0.42	0.30
enthalpy of vaporization (kJ mol^{-1})**	81	104	144	220

* NOTE: The fraction of free EC (not coordinated by Li^+) (Table S1) is determined by calculating the fraction of EC carbonyl oxygen atoms with an O-Li^+ distance > 2.8 Å. But approxiately 4.4% of the EC molecules are coordinated to Li^+ cations in the EC-LiTFSI 2-1 simulation via the etheral ring oxygen atoms (instead of the carbonyl oxygen atoms). For more dilute compositions, this percentage is much lower. This coordination is not reflected in the calculated fraction of coordinated and free EC molecules. Thus, the 14% value of uncoordinated EC molecules for the 2-1 composition in Table S1 is too high. It is unclear if the experimental analysis of the solvation numbers (Figure 1) would capture such coordination, however, as it is not known how this etheral ring oxygen coordination would affect the EC solvent Raman vibrational bands.

** The experimental molar enthalpy of vaporization for pure EC at 298.15 K is 60.81 kJ mol^{-1} and at 333.6 K is 59.13 kJ mol^{-1}.[1]

A simulation snapshot (extracted from the full simulation) for the EC-LiTFSI 10-1 mixture consists of a large number of uncoordinated $TFSI^-$ anions and a wide variety of solvates including fully solvated Li^+ cations (coordinated by four or five EC molecules), contact ion pairs (solvated Li^+TFSI^- pairs) and various small aggregates (Figures S9 and S10). A similar snapshot for the highly concentrated EC-LiTFSI 2-1 mixture (Figure S11) indicates that very few of the $TFSI^-$ anions are uncoordinated (to Li^+ cations). The are many more fully solvated Li^+ cations than uncoordinated anions because a number of the aggregate solvates have an extra $TFSI^-$ anion (i.e., are negatively charged). The relatively large number of fully solvated Li^+ cations coordinated by four or five EC molecules and contact ion pairs with Li^+ cations coordinated by three EC molecules, despite the overall concentration of 2-1, reflects the fact than many of the other Li^+ cations are coordinated by only a single EC molecule (as well as anions) or even fully coordinated by anions thereby making additional EC molecules available to coordinate the remaining Li^+ cations. Thus, many of the Li^+ cations serve as crosslink points resulting in the formation of very large aggregates which may consist of 100 or more Li^+ cations, $TFSI^-$ anions and EC molecules (Figure S11).

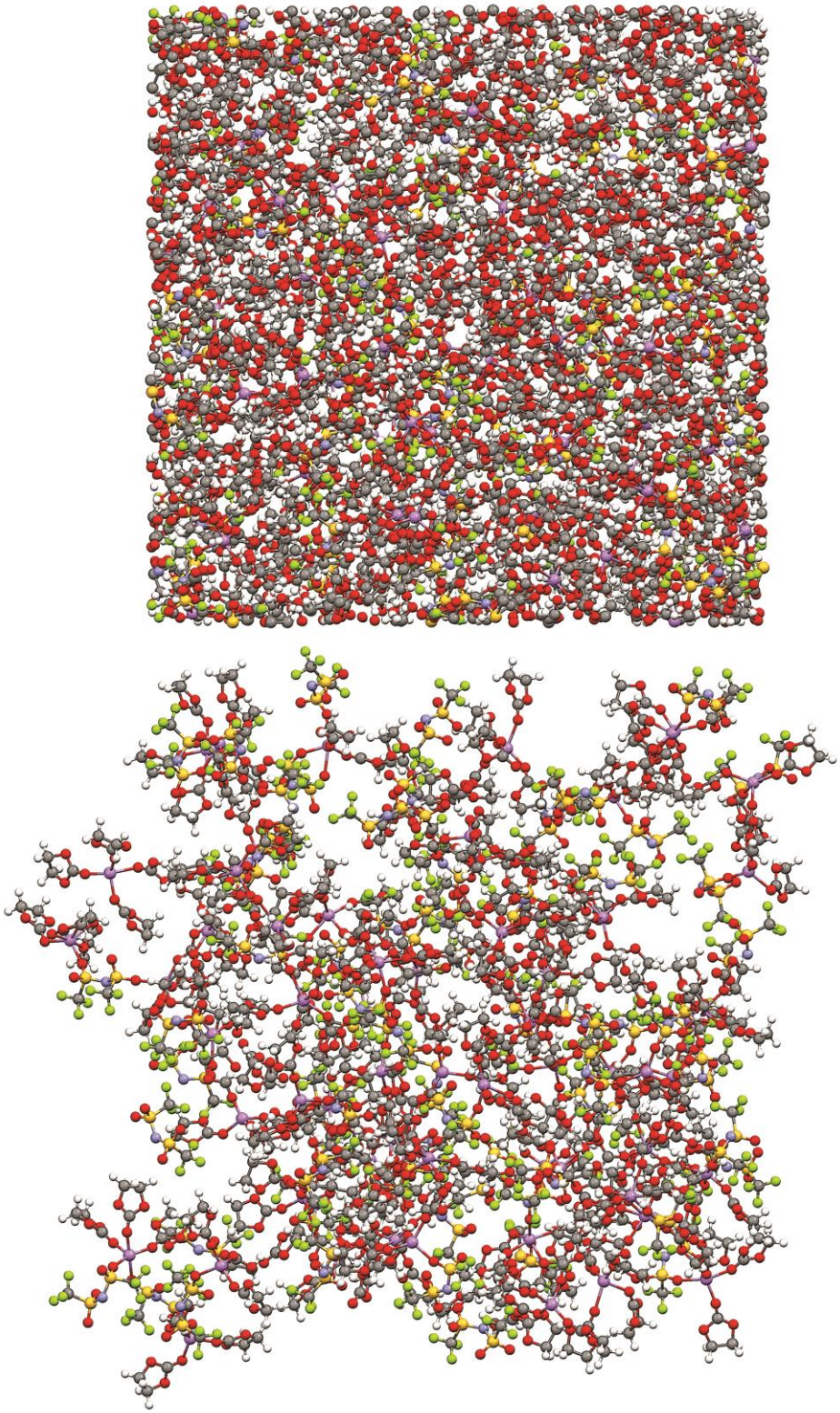

Figure S9. (top) Full MD simulation snapshot at 60°C for the EC-LiTFSI 10-1 mixture and (bottom) the same MD simulation snapshot with the uncoordinated EC molecules removed and the solvates grown across the periodic boundaries (Li-purple, O-red, N-blue, S-yellow, F-light green).

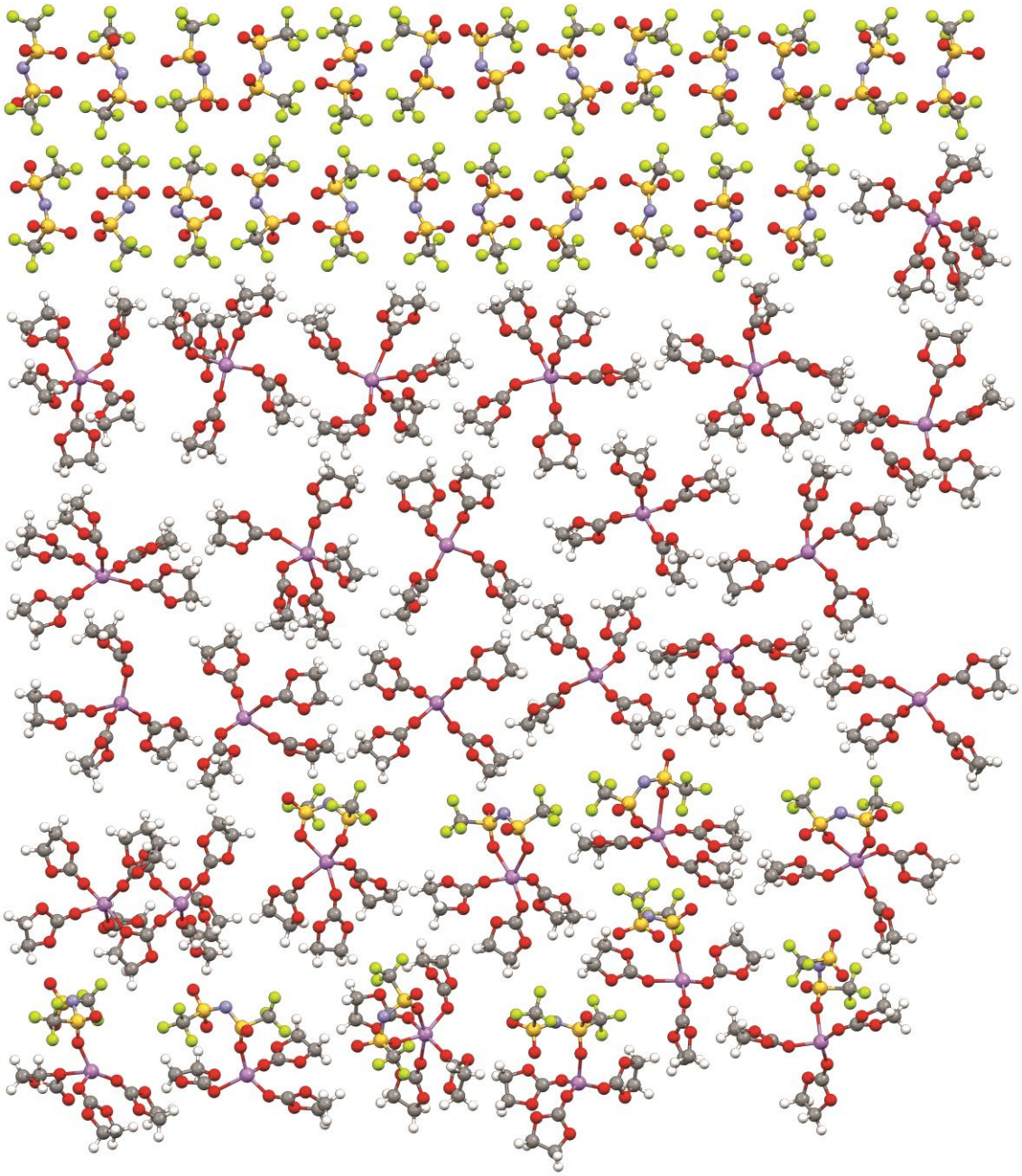

Figure S10. Visual list of individual anions and solvates extracted from the MD simulation at 60°C for the EC-LiTFSI 10-1 mixture (shown in Figure S9)—uncoordinated EC molecules not shown (Li-purple, O-red, N-blue, S-yellow, F-light green).

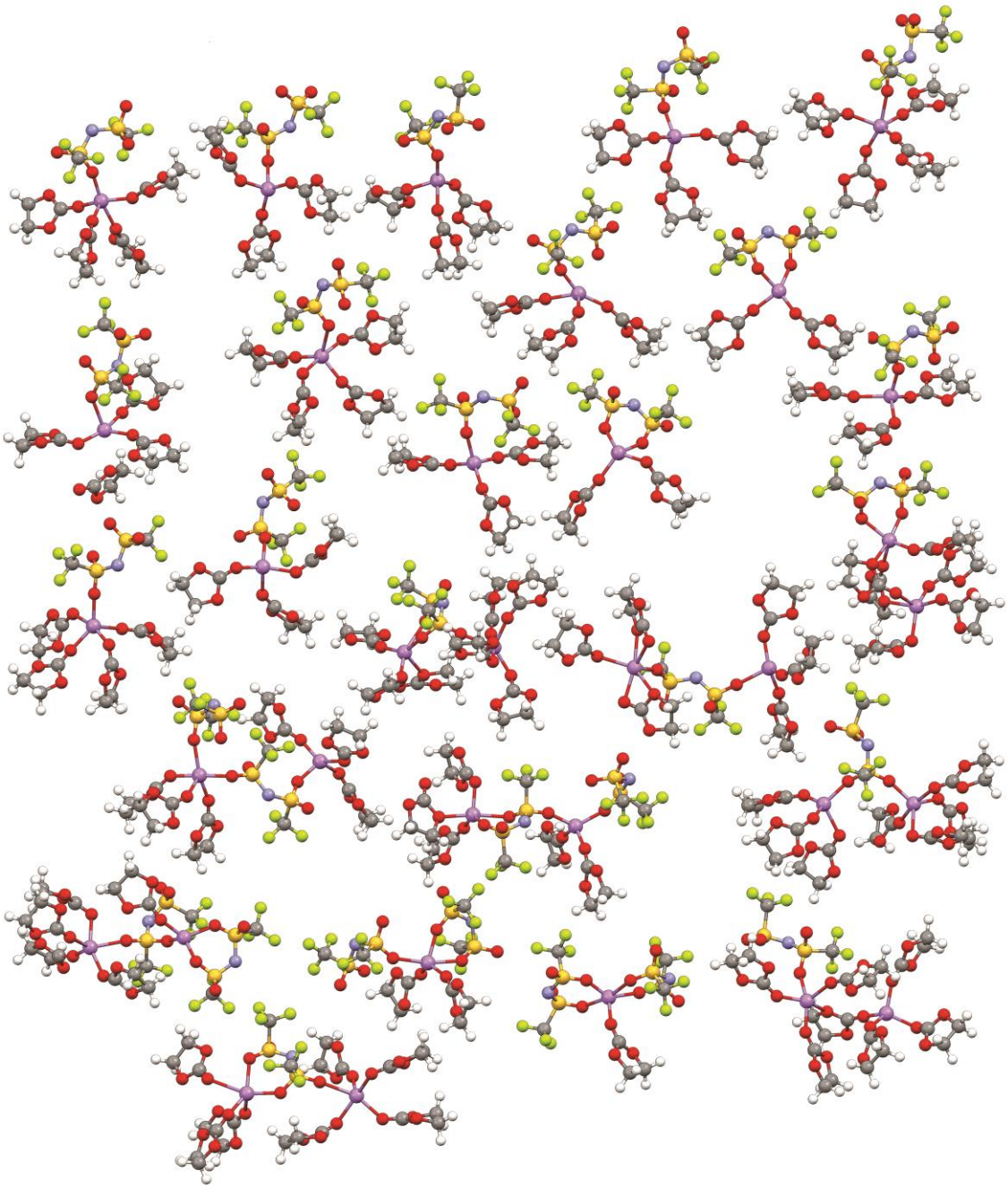

Figure S10 (cont). Visual list of individual anions and solvates extracted from the MD simulation at 60°C for the EC-LiTFSI 10-1 mixture (shown in Figure S9)—uncoordinated EC molecules not shown (Li-purple, O-red, N-blue, S-yellow, F-light green).

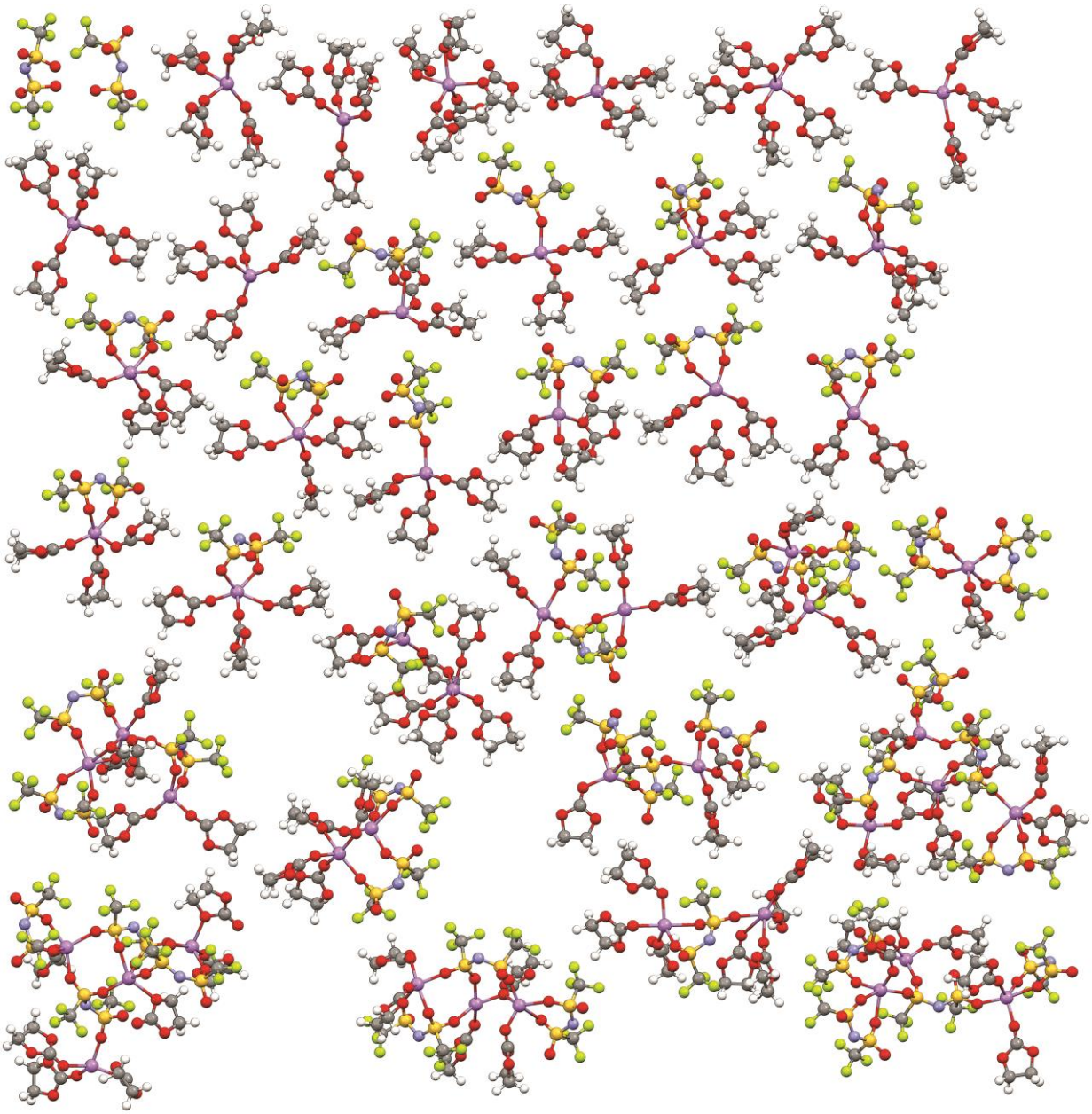

Figure S11. Visual list of individual anions and solvates extracted from the MD simulation at 60°C for the EC-LiTFSI 2-1 mixture—uncoordinated EC molecules not shown (Li-purple, O-red, N-blue, S-yellow, F-light green).

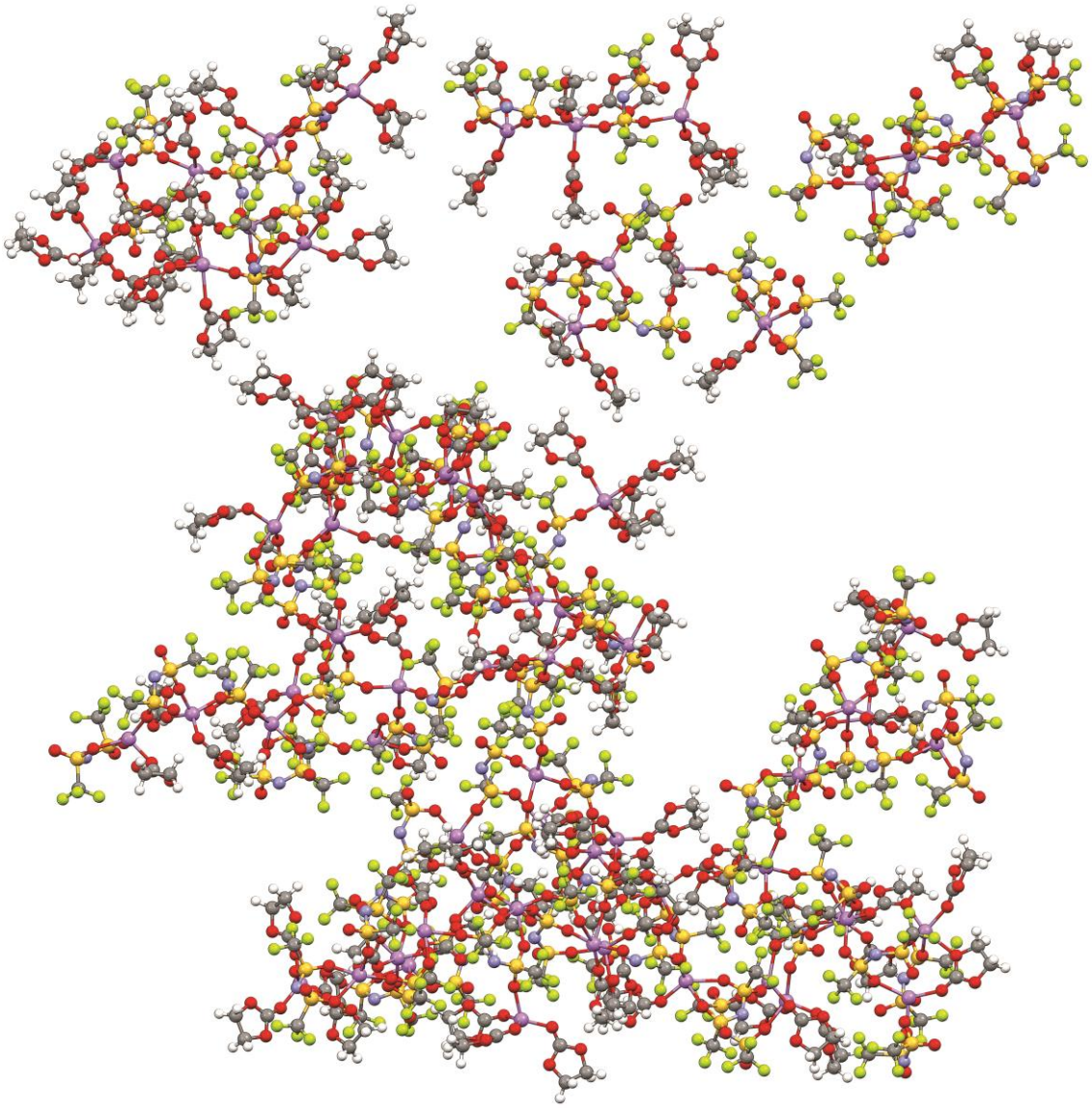

Figure S11 (cont). Visual list of individual anions and solvates extracted from the MD simulation at 60°C for the EC-LiTFSI 2-1 mixture—uncoordinated EC molecules not shown (Li-purple, O-red, N-blue, S-yellow, F-light green).

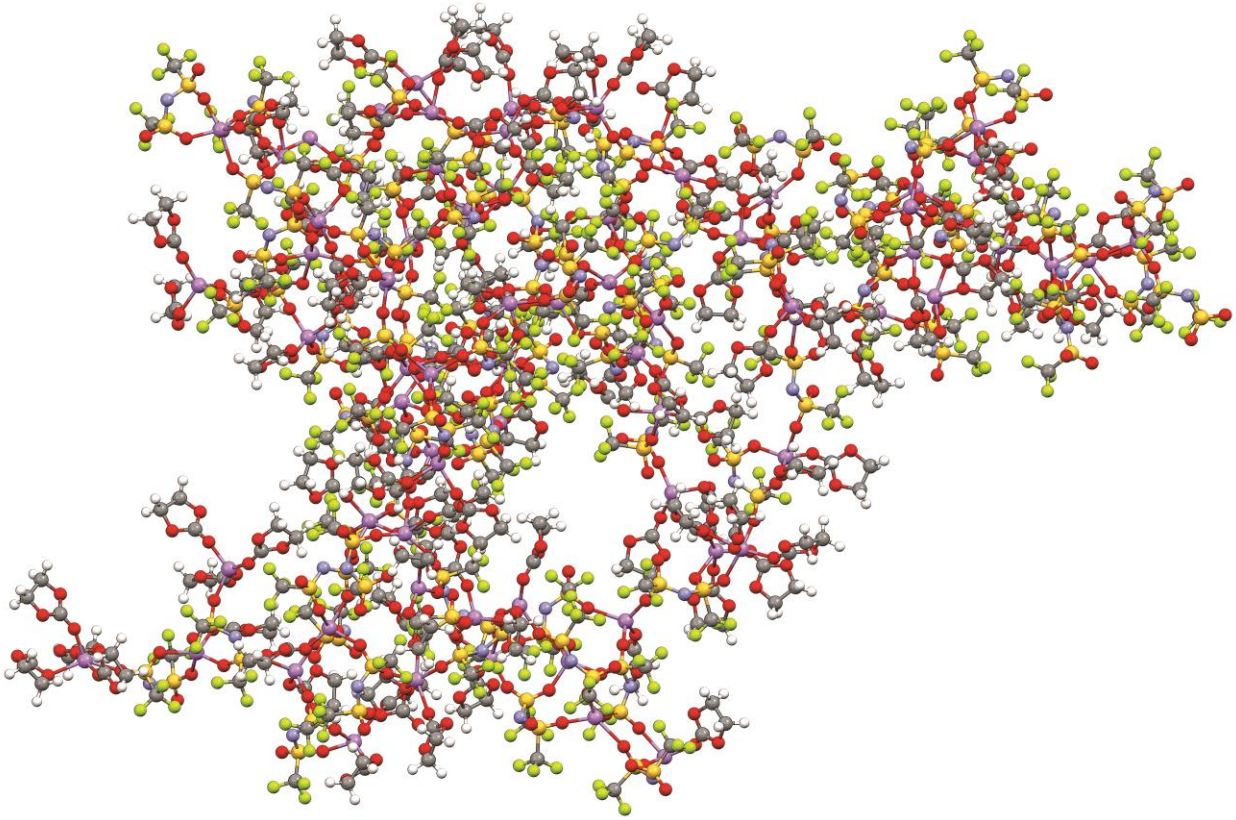

Figure S11 (cont). Visual list of individual anions and solvates extracted from the MD simulation at 60°C for the EC-LiTFSI 2-1 mixture—uncoordinated EC molecules not shown (Li-purple, O-red, N-blue, S-yellow, F-light green).

Quantum Chemistry Study of EC/TFSI$^-$ and EC/LiTFSI Oxidation

The initial stages of the oxidation induced reactions of [EC-TFSI$^-$] and [EC-Li$^+$-TFSI$^-$] complexes were studied using density functional calculations employing the M05-2X/6-31+G** level in order to understand the influence of a Li^+ cation on the oxidation stability of these complexes. The Gaussian g09 package was used with the SMD implicit solvent model developed by Marenich *et al.*[2,3] The absolute oxidation potential of a complex M relative to an electron at rest in vacuum ($E^0_{abs}(M)$) was calculated using Eq. 1:

$$E^o_{abs} = [\Delta G_e + \Delta G^0_S(M^+) - \Delta G^0_S(M)]/F \qquad (1)$$

where ΔG_e is the ionization free energy in the gas-phase at 298.15 K; $\Delta G_S(M^+)$ and $\Delta G_S(M)$ are the free energies of solvation of the oxidized and initial complexes M^+ and M, respectively, and F is Faraday's constant. Using the Li/Li^+ standard electrode potential of -3.05 V *vs* SHE for aqueous solutions,[4] a value of 4.42 - 3.05 = 1.37 V is obtained to convert the absolute potential scale E^o_{abs} to the Li/Li^+ scale in aqueous solutions from IUPAC recommendations as expressed by Eq. 2:

$$\Delta G^{ox} \text{ (}vs\text{ } Li^+/Li) = E^o_{abs} + E^o_{abs}(Li^+/Li) =$$
$$E°_{abs}\text{-}4.42 + 3.05 \text{ V} = E^0_{abs}\text{-}1.37 \text{ V} \approx E^0_{abs}\text{-}1.4 \text{ V} \qquad (2)$$

where E^o is the potential *vs* Li^+/Li.

The initial oxidation of the [EC-TFSI$^-$] complex (M0 in Figure S12) resulted in a M1 complex with an oxidation potential of 6.33 V *vs* Li^+/Li, which is significantly higher than the measured oxidation potential ~5.4 V for the 10-1 EC-LiTFSI concentration. Further investigation, however, revealed that there is a low barrier (~0.10 V, see TS1 - Figure S12) for the H-transfer reaction from EC to TFSI$^-$ for the oxidized [EC-TFSI$^-$] complex M2. Such H-transfer significantly reduces the oxidation stability of the [EC-TFSI$^-$] complex from 6.3 V to 5.3 V in agreement with previous studies of EC complexed with PF_6^-, BF_4^- and FSI^- anions.[5,6] A similar H-transfer reaction was found in EC_n (n = 2 and 4) clusters resulting in a slightly higher oxidation potential around 5.8-6.0 V as compared to the [EC-TFSI$^-$] reaction.[6,7]

The oxidative stability of the [EC-Li$^+$-TFSI$^-$] cluster was also calculated for two complexes with EC coordinated by a Li^+ cation (M4) and the TFSI$^-$ anion coordinating a Li^+ cation (M5) (relative to the M3 complex). EC polarization by a Li^+ cation increases the oxidative stability by 0.3 V. Interestingly, the TFSI$^-$ anion complexation to a Li^+ cation also increases the oxidative stability by a similar amount (~0.5 V). These calculations indicate that polarization of either the TFSI$^-$ anion or EC solvent molecule involved in the oxidation reaction increases the oxidation stability of the corresponding complex by 0.3-0.5 V.

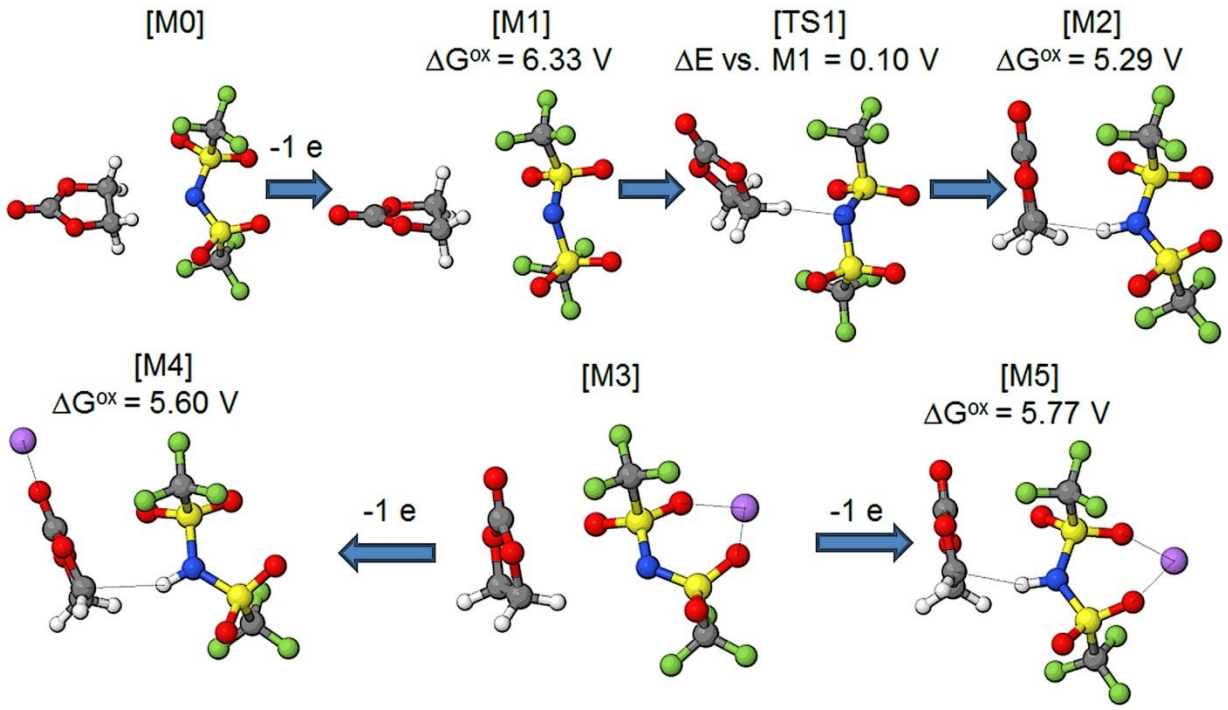

Figure S12. Oxidation-induced decomposition reactions of [EC-TFSI$^-$] and [EC-Li$^+$-TFSI$^-$]calculated at the M05-2X/6-31+G** level with SMD (EC, ε = 89.7, ε_{inf} = 2.05). Oxidation free energy (ΔG^{ox}) is given *vs* Li$^+$/Li.

MD Simulations of Charged Graphite-Electrolyte Interface

Figure S13 depicts the MD simulation results previously published[8] for the interface of a progressive charged graphite basal plane in contact with an electrolyte composed of an EC/DMC mixture with $LiPF_6$ (the overall electrolyte consisted of 114 EC molecules, 256 DMC molecules, 31 PF_6^- anions and 31 Li^+ cations). With increasing potential, the EC molecules replace the DMC molecules and PF_6^- anions displace the solvent molecules at the electrode surface. The EC molecules also realign so that both the carbonyl and one of the ring oxygen atoms are pointed at the surface (i.e., the electron lone-pairs are directed towards the positively charged surface).

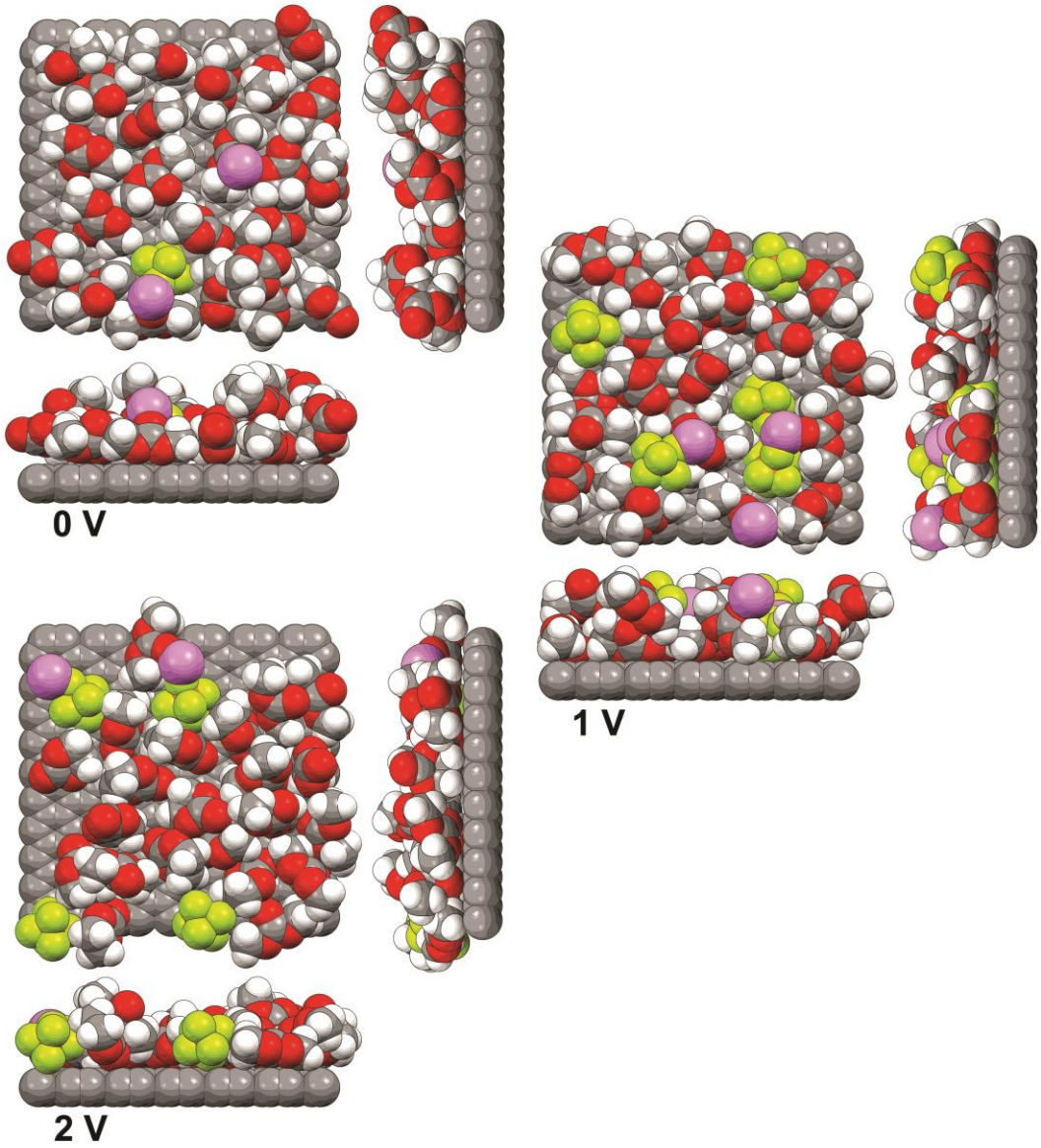

Figure S13. MD simulation snapshots of the graphite-electrolyte (EC/DMC-$LiPF_6$) interface as the electrode potential (between two graphite electrodes—with only the positively polarized electrode shown) is progressively increased (note that the boundaries are periodic) (Li-purple, C-gray, O-red, F-green) (three views—rotated 90°—shown for each potential).[8]

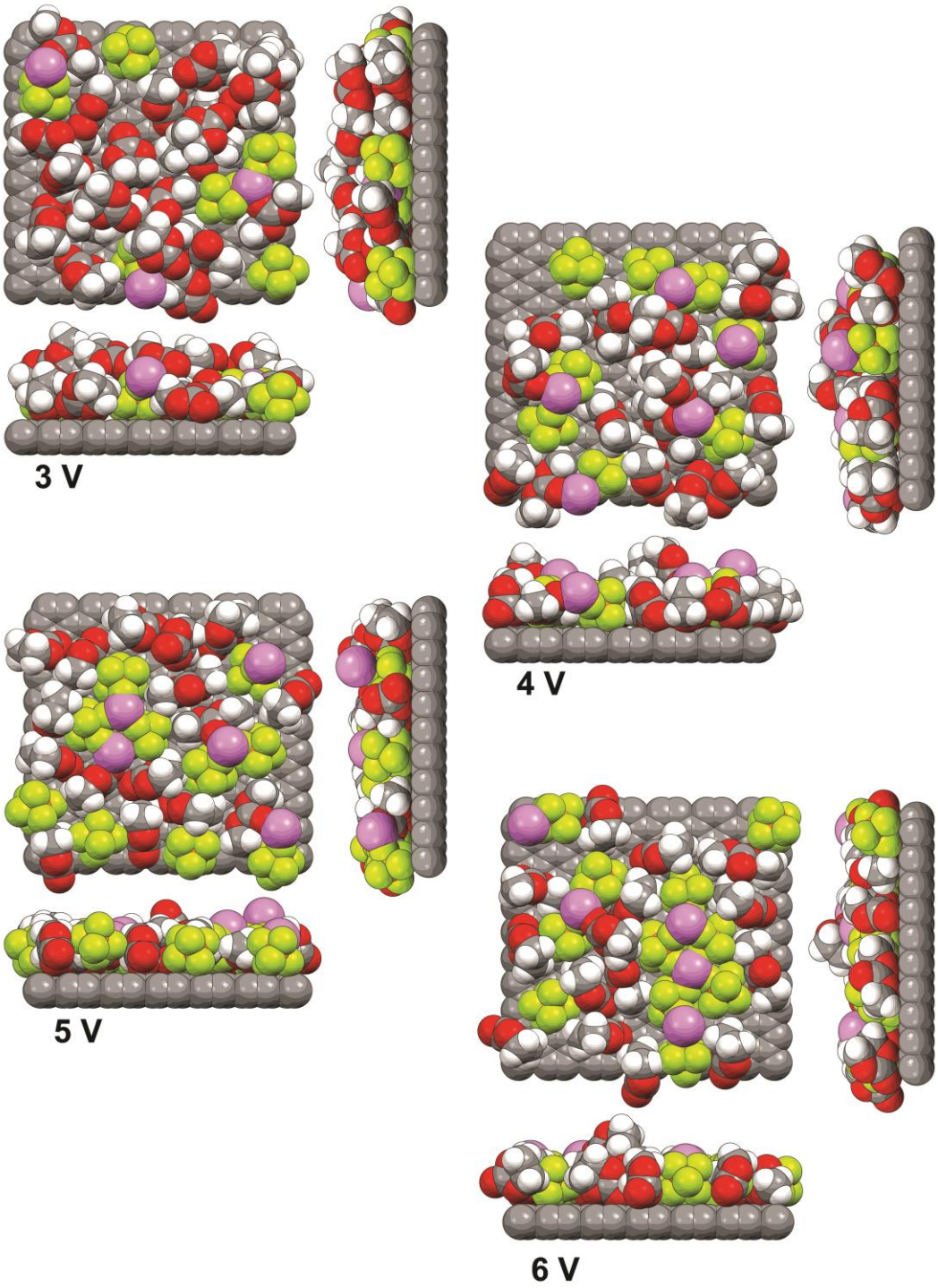

Figure S13 (cont). MD simulation snapshots of the graphite-electrolyte (EC/DMC-$LiPF_6$) interface as the electrode potential is progressively increased (note that the boundaries are periodic) (Li-purple, C-gray, O-red, F-green) (three views—rotated 90°—shown for each potential).[8]

Solvate Crystal Growth

$(EC)_1$:LiTFSI: Single crystals of the $(EC)_1$:LiTFSI solvate grew slowly from a 1.3-1 EC-LiTFSI mixture, prepared with EC (0.772 g, 8.2 mmol) and LiTFSI (1.811 g, 6.3 mmol), on storage at room temperature.

$(EC)_3$:LiTFSI: Single crystals of the $(EC)_3$:LiTFSI solvate grew slowly from a 4-1 EC-LiTFSI mixture, prepared with EC (0.793 g, 9.0 mmol) and LiTFSI (0.646 g, 2.3 mmol), on storage in a freezer at -23 °C.

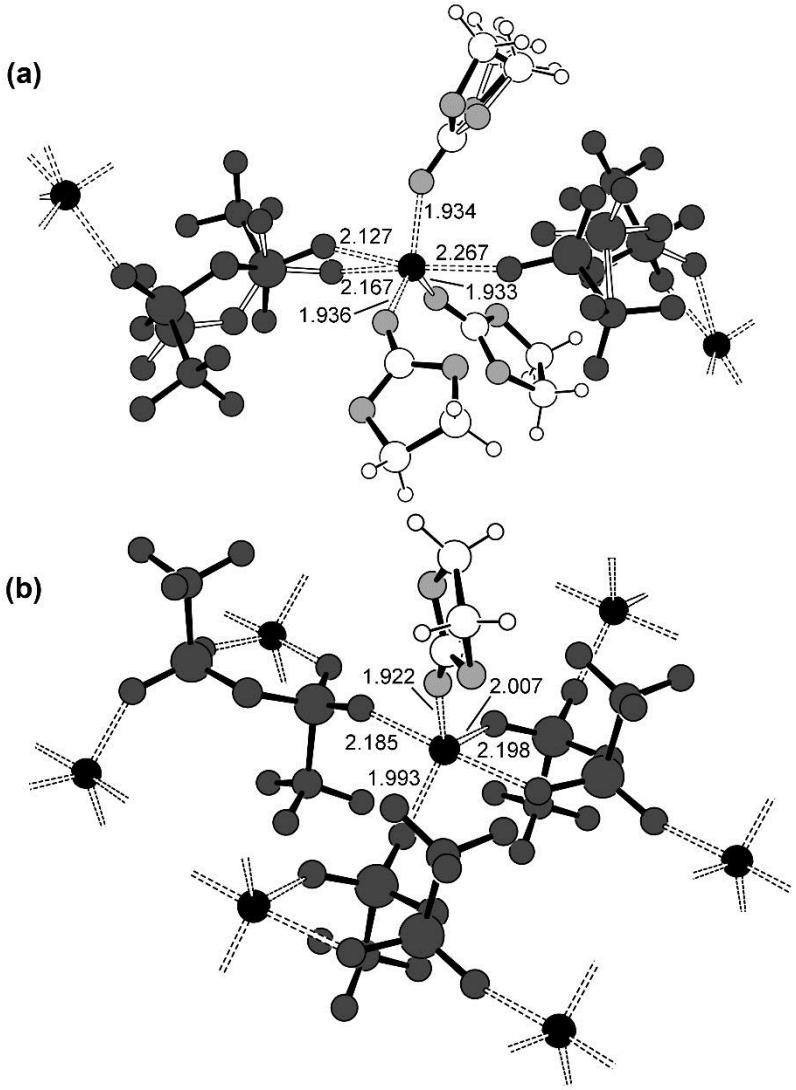

Figure S14. Coordination bond lengths (Å) in the $(EC)_3$:LiTFSI (disordered anions) and $(EC)_1$:LiTFSI crystalline solvates (black–Li^+ cations, light gray–solvent oxygen atoms, dark gray–anions).

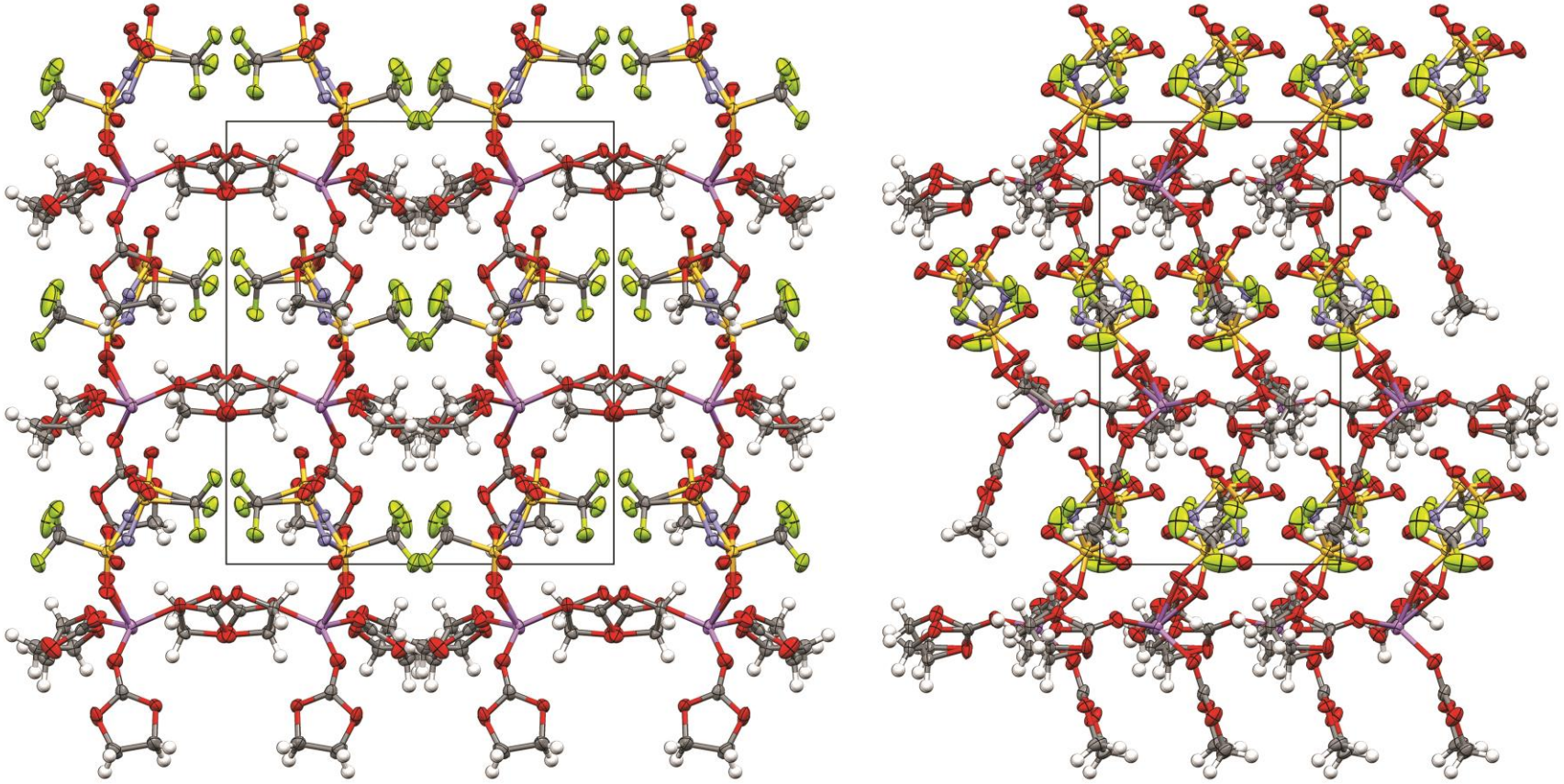

Figure S15. Ion packing within the crystal structure of the $(EC)_3$:LiTFSI solvate (two views) (Li-purple, O-red, N-blue, F-light green, S-gold).

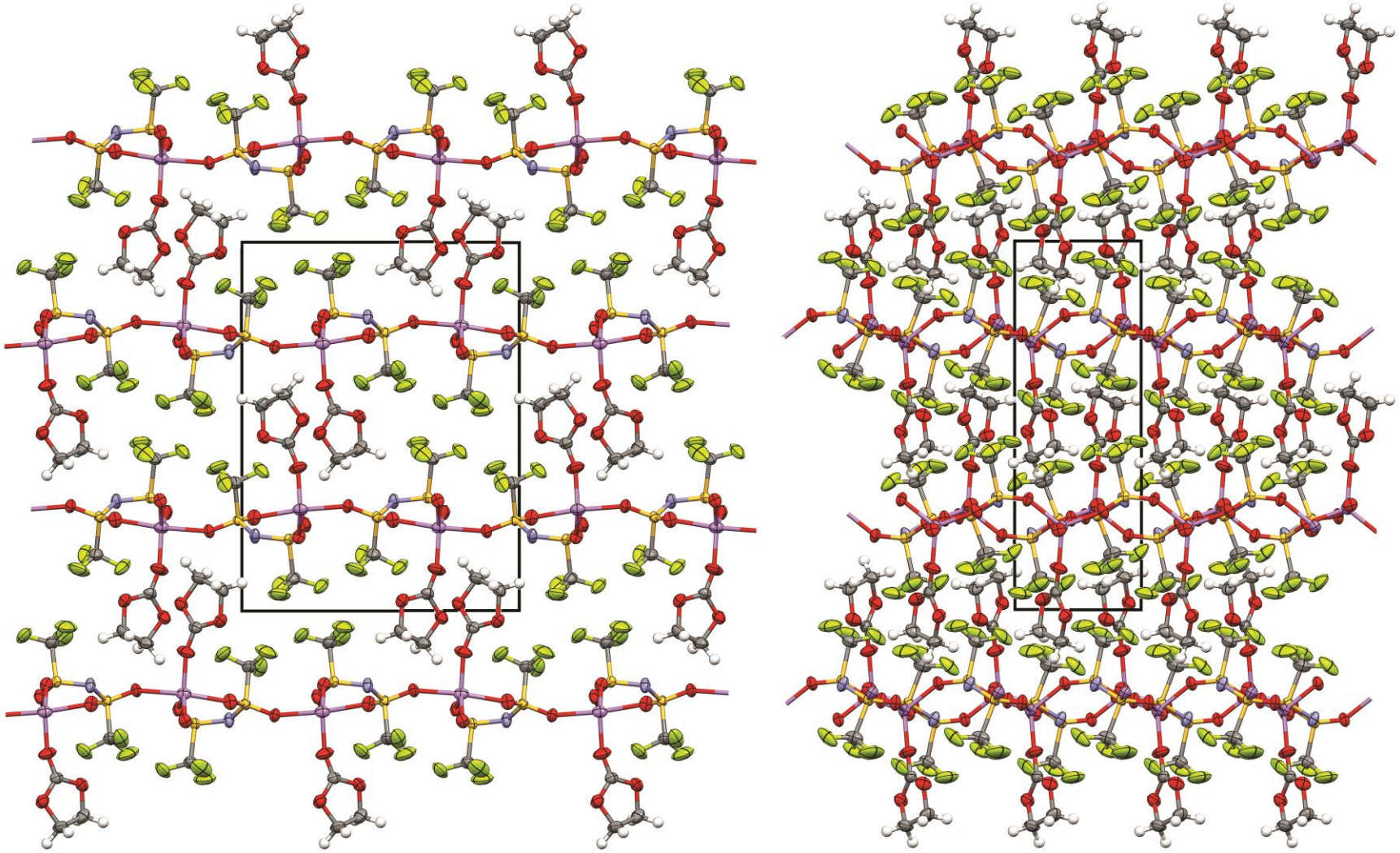

Figure S16. Ion packing within the crystal structure of the $(EC)_1$:LiTFSI solvate (two views) (Li-purple, O-red, N-blue, F-light green, S-gold).

$(EC)_3$:LiTFSI:

Data Collection and Processing. The sample was mounted on a Mitegen polyimide micromount with a small amount of Paratone N oil. All X-ray measurements were made on a Bruker-Nonius Kappa Axis X8 Apex2 diffractometer at a temperature of 110 K. The unit cell dimensions were determined from a symmetry constrained fit of 9791 reflections with 5.08° < 2θ < 59.68°. The data collection strategy was a number of ω and φ scans which collected data up to 75.64° (2θ). The frame integration was performed using SAINT.[9] The resulting raw data were scaled and absorption corrected using a multi-scan averaging of symmetry equivalent data using SADABS.[9]

Structure Solution and Refinement. The structure was solved by direct methods using the SIR92 program.[10] All non-hydrogen atoms were obtained from the initial solution. The hydrogen atoms were introduced at idealized positions and were allowed to ride on the parent atom. The structure exhibited two positional disorders, one in the anion and one in one of the coordinated solvents. The anion disorder resulted in distinct alternate positions for S1', O1', O2', N1', S2', O3', and O4'. The refined normalized occupancy for the predominant conformer was 0.9193(14). The coordinated solvent's disorder resulted in distinct alternate positions for O13', C11', and C10'. The refined occupancy for the unprimed sites was 0.472(3). The structural model was fit to the data using full matrix least-squares based on F^2. The calculated structure factors included corrections for anomalous dispersion from the usual tabulation. The calculated structure factors included corrections for anomalous dispersion from the usual tabulation. The structure was refined using the XL program from SHELXTL.[11] Graphic plots were produced using the NRCVAX crystallographic program suite.[12]

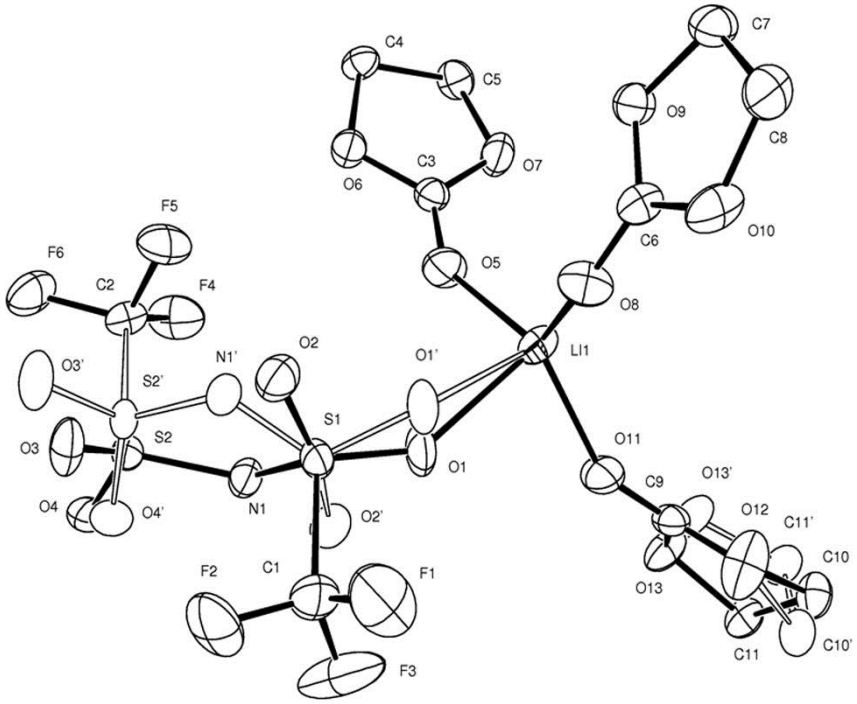

Figure S17. ORTEP drawing of $(EC)_3$:LiTFSI showing naming and numbering scheme. Note the two molecules in the asymmetric unit. Ellipsoids are at the 50% probability level and hydrogen atoms were drawn with arbitrary radii for clarity.

Table S2. Summary of Crystal Data for $(EC)_3$:LiTFSI

formula	$C_{11}H_{12}F_6LiNO_{13}S_2$
formula weight (g mol^{-1})	551.28
crystal dimensions (mm)	0.56 × 0.22 × 0.16
crystal color and habit	colourless prism
crystal system	orthorhombic
space group	P $ca2_1$
temperature (K)	110
a (Å)	8.729(3)
b (Å)	14.045(5)
c (Å)	16.041(6)
α (°)	90.00
β (°)	90.00
γ (°)	90.00
V ($Å^3$)	1966.5(12)
number of reflections to determine final unit cell	9791
min and max 2θ for cell determination (°)	5.08, 59.68
Z	4
F(000)	1112
ρ (g cm^{-3})	1.862
λ (Å) (MoKα)	0.71073
μ (cm^{-1})	0.397
diffractometer type	Bruker-Nonius Kappa Axis X8 Apex2
scan type (s)	omega and phi scans
max 2θ for data collection (°)	75.64
measured fraction of data	0.998
number of reflections measured	133179
unique reflections measured	10519
R_{merge}	0.0400
number of reflections included in refinement	10519
cut off threshold expression	>2sigma(I)
structure refined using	full matrix least-squares using F^2
weighting scheme	calc w=1/[$sigma^2(Fo^2)$+(0.0674P)^2+ 0.5247P] where P=(Fo^2+2Fc^2)/3
number of parameters in least-squares	344
R_1	0.0472
wR_2	0.1138
R_1 (all data)	0.0730
wR_2 (all data)	0.1265
GOF	1.022
maximum shift/error	0.000
min & max peak heights on final ΔF Map (e^- $Å^{-1}$)	-0.524, 0.691

$R_1 = \Sigma(|F_o| - |F_c|)/\Sigma F_o$

$wR_2 = [\Sigma(w(F_o^2 - F_c^2)^2)/\Sigma(w F_o^4)]^{1/2}$

GOF = $[\Sigma(w(F_o^2 - F_c^2)^2)/(\text{No. of reflns. - No. of params.})]^{1/2}$

Table S3. Atomic Coordinates for $(EC)_3$:LiTFSI

Atom	x	y	z	$U_{iso/equiv}$
Li1	0.2367(3)	0.2454(2)	0.6412(2)	0.0260(5)
S1	0.44753(5)	0.30619(3)	0.47116(3)	0.02507(8)
O1	0.3297(2)	0.30930(12)	0.53216(11)	0.0377(4)
O2	0.60145(19)	0.28307(12)	0.49721(10)	0.0334(3)
S2	0.49311(5)	0.20231(3)	0.32483(3)	0.02164(9)
O3	0.64837(17)	0.23573(11)	0.32005(11)	0.0341(3)
O4	0.4093(2)	0.19352(11)	0.24897(10)	0.0345(3)
N1	0.38694(18)	0.25149(11)	0.39196(11)	0.0246(3)
C1	0.4605(3)	0.43008(15)	0.43600(16)	0.0395(4)
F1	0.4995(4)	0.48575(12)	0.49735(13)	0.0827(7)
F2	0.5614(2)	0.43923(11)	0.37638(11)	0.0553(4)
F3	0.3279(2)	0.45842(13)	0.40527(19)	0.0806(7)
C2	0.50969(19)	0.08007(12)	0.36239(12)	0.0259(3)
F4	0.37286(15)	0.04088(10)	0.37076(10)	0.0439(3)
F5	0.58239(17)	0.07414(10)	0.43432(8)	0.0393(3)
F6	0.58731(17)	0.02989(9)	0.30565(9)	0.0402(3)
S1'	0.44753(5)	0.30619(3)	0.47116(3)	0.02507(8)
O1'	0.411(3)	0.3080(14)	0.5624(13)	0.0377(4)
O2'	0.288(2)	0.3047(13)	0.4270(12)	0.0334(3)
S2'	0.5799(5)	0.2122(3)	0.3550(3)	0.0177(10)
O3'	0.739(2)	0.2031(12)	0.3369(12)	0.0341(3)
O4'	0.479(2)	0.2460(14)	0.2907(11)	0.0345(3)
N1'	0.5794(18)	0.2536(12)	0.4444(10)	0.0246(3)
C1'	0.4605(3)	0.43008(15)	0.43600(16)	0.0395(4)
F1'	0.4995(4)	0.48575(12)	0.49735(13)	0.0827(7)
F2'	0.5614(2)	0.43923(11)	0.37638(11)	0.0553(4)
F3'	0.3279(2)	0.45842(13)	0.40527(19)	0.0806(7)
C2'	0.50969(19)	0.08007(12)	0.36239(12)	0.0259(3)
F4'	0.37286(15)	0.04088(10)	0.37076(10)	0.0439(3)
F5'	0.58239(17)	0.07414(10)	0.43432(8)	0.0393(3)
F6'	0.58731(17)	0.02989(9)	0.30565(9)	0.0402(3)
O5	0.2538(2)	0.11932(9)	0.59336(9)	0.0379(3)
C3	0.2475(2)	0.03473(12)	0.60552(10)	0.0242(3)
O6	0.33359(16)	-0.02709(9)	0.56540(9)	0.0283(2)
O7	0.15432(18)	-0.00670(11)	0.66006(10)	0.0362(3)
C4	0.31035(19)	-0.12131(11)	0.59949(11)	0.0253(3)
C5	0.1688(2)	-0.10939(13)	0.65292(12)	0.0289(3)
O8	0.38999(17)	0.28783(11)	0.71987(10)	0.0347(3)
C6	0.43084(19)	0.26918(12)	0.79011(12)	0.0265(3)
O9	0.44176(17)	0.18233(9)	0.81986(9)	0.0300(3)
O10	0.47313(18)	0.33552(10)	0.84473(12)	0.0390(4)
C7	0.4894(3)	0.18555(16)	0.90590(14)	0.0388(5)
C8	0.5200(3)	0.29016(18)	0.92186(15)	0.0394(5)
O11	0.07083(18)	0.33477(14)	0.62474(11)	0.0418(4)
C9	-0.04605(17)	0.37255(11)	0.64728(10)	0.0249(3)
O12	-0.05185(14)	0.45246(13)	0.68969(13)	0.0463(4)
O13	-0.1792(4)	0.3490(3)	0.6129(2)	0.0313(6)
C10'	-0.2091(4)	0.4895(3)	0.6875(3)	0.0292(7)
C11	-0.2898(4)	0.4208(2)	0.6393(2)	0.0269(4)

O11'	0.07083(18)	0.33477(14)	0.62474(11)	0.0418(4)
C9'	-0.04605(17)	0.37255(11)	0.64728(10)	0.0249(3)
O12'	-0.05185(14)	0.45246(13)	0.68969(13)	0.0463(4)
O13'	-0.1835(3)	0.3326(2)	0.6475(2)	0.0313(6)
C10	-0.2125(4)	0.4648(3)	0.7136(2)	0.0292(7)
C11'	-0.2905(3)	0.3944(2)	0.6902(2)	0.0269(4)
H4A	0.3993	-0.1415	0.6335	0.030
H4B	0.2930	-0.1686	0.5547	0.030
H5A	0.0777	-0.1375	0.6256	0.035
H5B	0.1827	-0.1393	0.7083	0.035
H7A	0.5833	0.1473	0.9146	0.047
H7B	0.4077	0.1614	0.9431	0.047
H8A	0.4587	0.3137	0.9695	0.047
H8B	0.6299	0.3016	0.9333	0.047
H10A	-0.2524	0.4944	0.7444	0.035
H10B	-0.2127	0.5530	0.6607	0.035
H11A	-0.3373	0.4514	0.5900	0.032
H11B	-0.3718	0.3910	0.6731	0.032
H10C	-0.2201	0.4716	0.7749	0.035
H10D	-0.2535	0.5236	0.6879	0.035
H11C	-0.3735	0.4148	0.6521	0.032
H11D	-0.3365	0.3614	0.7387	0.032

Table S4. Anisotropic Displacement Parameters for $(EC)_3$:LiTFSI

Atom	u^{11}	u^{22}	u^{33}	u^{12}	u^{13}	u^{23}
Li1	0.0238(12)	0.0207(12)	0.0333(14)	0.0032(10)	-0.0043(11)	-0.0043(11)
S1	0.03163(19)	0.02197(15)	0.02161(15)	0.00032(13)	0.00708(14)	0.00154(14)
O1	0.0453(9)	0.0363(8)	0.0314(8)	0.0013(7)	0.0223(7)	-0.0009(6)
O2	0.0349(7)	0.0346(7)	0.0307(7)	0.0084(6)	-0.0041(6)	-0.0056(6)
S2	0.02466(19)	0.01922(15)	0.02104(16)	0.00238(13)	0.00463(15)	0.00098(15)
O3	0.0319(6)	0.0297(6)	0.0408(8)	-0.0069(5)	0.0180(7)	-0.0097(6)
O4	0.0484(9)	0.0330(7)	0.0221(6)	0.0140(6)	-0.0036(6)	0.0031(5)
N1	0.0229(6)	0.0241(6)	0.0268(6)	0.0031(5)	0.0042(5)	-0.0013(5)
C1	0.0482(12)	0.0241(8)	0.0463(11)	0.0019(8)	0.0092(9)	0.0056(8)
F1	0.166(2)	0.0303(8)	0.0517(10)	-0.0160(10)	0.0131(12)	-0.0134(7)
F2	0.0807(12)	0.0377(7)	0.0476(8)	-0.0222(7)	0.0185(8)	0.0063(6)
F3	0.0603(11)	0.0403(8)	0.141(2)	0.0146(8)	-0.0119(12)	0.0300(11)
C2	0.0255(7)	0.0219(7)	0.0303(8)	0.0034(5)	-0.0054(6)	0.0014(6)
F4	0.0328(6)	0.0384(6)	0.0606(9)	-0.0103(5)	-0.0072(6)	0.0149(6)
F5	0.0444(7)	0.0394(6)	0.0341(6)	0.0026(5)	-0.0159(5)	0.0052(5)
F6	0.0473(7)	0.0273(5)	0.0459(7)	0.0105(5)	-0.0043(6)	-0.0084(5)
S1'	0.03163(19)	0.02197(15)	0.02161(15)	0.00032(13)	0.00708(14)	0.00154(14)
O1'	0.0453(9)	0.0363(8)	0.0314(8)	0.0013(7)	0.0223(7)	-0.0009(6)
O2'	0.0349(7)	0.0346(7)	0.0307(7)	0.0084(6)	-0.0041(6)	-0.0056(6)
S2'	0.0132(17)	0.0216(19)	0.0183(18)	-0.0015(13)	0.0032(14)	-0.0032(14)
O3'	0.0319(6)	0.0297(6)	0.0408(8)	-0.0069(5)	0.0180(7)	-0.0097(6)
O4'	0.0484(9)	0.0330(7)	0.0221(6)	0.0140(6)	-0.0036(6)	0.0031(5)
N1'	0.0229(6)	0.0241(6)	0.0268(6)	0.0031(5)	0.0042(5)	-0.0013(5)
C1'	0.0482(12)	0.0241(8)	0.0463(11)	0.0019(8)	0.0092(9)	0.0056(8)
F1'	0.166(2)	0.0303(8)	0.0517(10)	-0.0160(10)	0.0131(12)	-0.0134(7)

F2'	0.0807(12)	0.0377(7)	0.0476(8)	-0.0222(7)	0.0185(8)	0.0063(6)
F3'	0.0603(11)	0.0403(8)	0.141(2)	0.0146(8)	-0.0119(12)	0.0300(11)
C2'	0.0255(7)	0.0219(7)	0.0303(8)	0.0034(5)	-0.0054(6)	0.0014(6)
F4'	0.0328(6)	0.0384(6)	0.0606(9)	-0.0103(5)	-0.0072(6)	0.0149(6)
F5'	0.0444(7)	0.0394(6)	0.0341(6)	0.0026(5)	-0.0159(5)	0.0052(5)
F6'	0.0473(7)	0.0273(5)	0.0459(7)	0.0105(5)	-0.0043(6)	-0.0084(5)
O5	0.0620(9)	0.0187(5)	0.0329(6)	0.0032(6)	-0.0018(7)	-0.0015(5)
C3	0.0294(7)	0.0221(6)	0.0212(6)	0.0026(5)	-0.0034(5)	-0.0004(5)
O6	0.0339(6)	0.0179(5)	0.0330(6)	0.0001(4)	0.0112(5)	0.0047(4)
O7	0.0395(7)	0.0313(7)	0.0376(7)	0.0076(6)	0.0150(6)	0.0012(6)
C4	0.0236(6)	0.0182(6)	0.0340(8)	0.0008(5)	0.0014(5)	0.0039(6)
C5	0.0265(7)	0.0283(7)	0.0319(8)	-0.0053(6)	0.0052(6)	0.0056(6)
O8	0.0305(6)	0.0351(7)	0.0383(7)	-0.0076(5)	-0.0127(6)	0.0054(6)
C6	0.0218(6)	0.0228(7)	0.0351(8)	-0.0003(5)	-0.0072(6)	-0.0029(6)
O9	0.0400(7)	0.0228(5)	0.0273(6)	0.0021(4)	-0.0062(5)	-0.0046(5)
O10	0.0414(7)	0.0223(6)	0.0533(9)	0.0027(5)	-0.0195(6)	-0.0119(6)
C7	0.0512(12)	0.0340(10)	0.0312(9)	0.0117(8)	-0.0143(8)	-0.0035(8)
C8	0.0413(10)	0.0406(11)	0.0363(10)	0.0032(8)	-0.0134(8)	-0.0125(8)
O11	0.0314(7)	0.0540(9)	0.0401(8)	0.0222(6)	0.0086(6)	0.0176(7)
C9	0.0212(6)	0.0280(7)	0.0256(7)	0.0050(5)	0.0001(5)	0.0085(6)
O12	0.0167(5)	0.0589(10)	0.0633(11)	-0.0064(6)	-0.0022(6)	-0.0271(9)
O13	0.0260(7)	0.0245(11)	0.0433(17)	0.0046(7)	-0.0092(12)	-0.0108(12)
C10'	0.0212(8)	0.037(2)	0.0296(19)	0.0011(11)	0.0004(12)	-0.0058(13)
C11	0.0153(7)	0.0281(11)	0.0374(11)	0.0021(7)	-0.0009(9)	-0.0018(9)
O11'	0.0314(7)	0.0540(9)	0.0401(8)	0.0222(6)	0.0086(6)	0.0176(7)
C9'	0.0212(6)	0.0280(7)	0.0256(7)	0.0050(5)	0.0001(5)	0.0085(6)
O12'	0.0167(5)	0.0589(10)	0.0633(11)	-0.0064(6)	-0.0022(6)	-0.0271(9)
O13'	0.0260(7)	0.0245(11)	0.0433(17)	0.0046(7)	-0.0092(12)	-0.0108(12)
C10	0.0212(8)	0.037(2)	0.0296(19)	0.0011(11)	0.0004(12)	-0.0058(13)
C11'	0.0153(7)	0.0281(11)	0.0374(11)	0.0021(7)	-0.0009(9)	-0.0018(9)

Table S5. Bond Lengths for $(EC)_3$:LiTFSI

Li1-O8	1.933(3)	C4-H4A	0.9900
Li1-O11	1.934(3)	C4-H4B	0.9900
Li1-O5	1.936(3)	C5-H5A	0.9900
Li1-O1	2.127(4)	C5-H5B	0.9900
Li1-O1'	2.167(19)	O8-C6	1.210(2)
Li1-O4[1]	2.267(4)	C6-O9	1.313(2)
S1-O1	1.4203(15)	C6-O10	1.331(2)
S1-O2	1.4440(17)	O9-C7	1.442(3)
S1-N1	1.5760(18)	O10-C8	1.450(3)
S1-C1	1.833(2)	C7-C8	1.515(3)
S2-O4	1.4254(17)	C7-H7A	0.9900
S2-O3	1.4363(16)	C7-H7B	0.9900
S2-N1	1.5797(16)	C8-H8A	0.9900
S2-C2	1.8252(19)	C8-H8B	0.9900
O4-Li1[2]	2.267(4)	O11-C9	1.205(2)
C1-F1	1.302(3)	C9-O12	1.313(2)
C1-F2	1.306(3)	C9-O13	1.328(3)
C1-F3	1.320(3)	O12-C10'	1.469(4)

C2-F5	1.319(2)	O13-C11	1.458(4)
C2-F4	1.322(2)	C10'-C11	1.424(6)
C2-F6	1.336(2)	C10'-H10A	0.9900
S2'-O3'	1.425(18)	C10'-H10B	0.9900
S2'-O4'	1.435(18)	C11-H11A	0.9900
S2'-N1'	1.547(14)	C11-H11B	0.9900
O5-C3	1.205(2)	O13'-C11'	1.448(3)
C3-O6	1.316(2)	C10-C11'	1.258(5)
C3-O7	1.329(2)	C10-H10C	0.9900
O6-C4	1.4462(19)	C10-H10D	0.9900
O7-C5	1.452(2)	C11'-H11C	0.9900
C4-C5	1.513(2)	C11'-H11D	0.9900

1. -x+1/2, y, z+1/2
2. -x+1/2, y,-1+ z+1/2

Table S6. Bond Angles for $(EC)_3$:LiTFSI

O8-Li1-O11	114.06(17)	O6-C4-H4B	111.1
O8-Li1-O5	119.17(17)	C5-C4-H4B	111.1
O11-Li1-O5	126.64(18)	H4A-C4-H4B	109.1
O8-Li1-O1	98.21(16)	O7-C5-C4	103.04(13)
O11-Li1-O1	84.22(15)	O7-C5-H5A	111.2
O5-Li1-O1	91.72(15)	C4-C5-H5A	111.2
O8-Li1-O1'	76.6(7)	O7-C5-H5B	111.2
O11-Li1-O1'	100.6(6)	C4-C5-H5B	111.2
O5-Li1-O1'	94.9(5)	H5A-C5-H5B	109.1
O1-Li1-O1'	23.1(7)	C6-O8-Li1	138.13(17)
O8-Li1-O4[1]	89.47(15)	O8-C6-O9	124.10(17)
O11-Li1-O4[1]	83.81(14)	O8-C6-O10	122.87(18)
O5-Li1-O4[1]	92.95(15)	O9-C6-O10	113.01(17)
O1-Li1-O4[1]	167.65(17)	C6-O9-C7	109.85(15)
O1'-Li1-O4[1]	166.1(7)	C6-O10-C8	109.40(16)
O1-S1-O2	118.78(12)	O9-C7-C8	104.06(18)
O1-S1-N1	109.11(11)	O9-C7-H7A	110.9
O2-S1-N1	115.85(9)	C8-C7-H7A	110.9
O1-S1-C1	103.14(10)	O9-C7-H7B	110.9
O2-S1-C1	104.19(11)	C8-C7-H7B	110.9
N1-S1-C1	103.62(11)	H7A-C7-H7B	109.0
S1-O1-Li1	146.09(15)	O10-C8-C7	103.43(16)
O4-S2-O3	117.85(11)	O10-C8-H8A	111.1
O4-S2-N1	108.58(10)	C7-C8-H8A	111.1
O3-S2-N1	116.55(9)	O10-C8-H8B	111.1
O4-S2-C2	103.95(9)	C7-C8-H8B	111.1
O3-S2-C2	104.49(9)	H8A-C8-H8B	109.0
N1-S2-C2	103.46(9)	C9-O11-Li1	151.40(18)
S2-O4-Li1[2]	155.69(13)	O11-C9-O12	124.34(18)
S1-N1-S2	124.45(11)	O11-C9-O13	120.4(2)
F1-C1-F2	108.5(2)	O12-C9-O13	113.21(19)
F1-C1-F3	109.3(2)	C9-O12-C10'	109.1(2)
F2-C1-F3	106.7(2)	C9-O13-C11	106.7(3)
F1-C1-S1	110.71(18)	C11-C10'-O12	103.6(3)

F2-C1-S1	111.12(16)	C11-C10'-H10A	111.0
F3-C1-S1	110.32(17)	O12-C10'-H10A	111.0
F5-C2-F4	108.63(17)	C11-C10'-H10B	111.0
F5-C2-F6	108.58(15)	O12-C10'-H10B	111.0
F4-C2-F6	107.93(16)	H10A-C10'-H10B	109.0
F5-C2-S2	112.71(13)	C10'-C11-O13	107.4(3)
F4-C2-S2	110.70(12)	C10'-C11-H11A	110.2
F6-C2-S2	108.16(13)	O13-C11-H11A	110.2
O3'-S2'-O4'	118.8(12)	C10'-C11-H11B	110.2
O3'-S2'-N1'	103.0(10)	O13-C11-H11B	110.2
O4'-S2'-N1'	122.6(10)	H11A-C11-H11B	108.5
C3-O5-Li1	146.50(17)	C11'-C10-H10C	109.6
O5-C3-O6	123.01(17)	C11'-C10-H10D	109.6
O5-C3-O7	124.50(17)	H10C-C10-H10D	108.1
O6-C3-O7	112.49(15)	C10-C11'-O13'	105.3(3)
C3-O6-C4	109.78(13)	C10-C11'-H11C	110.7
C3-O7-C5	109.25(14)	O13'-C11'-H11C	110.7
O6-C4-C5	103.15(13)	C10-C11'-H11D	110.7
O6-C4-H4A	111.1	O13'-C11'-H11D	110.7
C5-C4-H4A	111.1	H11C-C11'-H11D	108.8

1. -x+1/2, y, z+1/2
2. -x+1/2, y,-1+ z+1/2

Table S7. Torsion Angles for $(EC)_3$:LiTFSI

O2-S1-O1-Li1	-39.5(3)	$O4^1$-Li1-O5-C3	-22.5(3)
N1-S1-O1-Li1	96.3(3)	Li1-O5-C3-O6	-146.7(3)
C1-S1-O1-Li1	-154.0(3)	Li1-O5-C3-O7	33.3(4)
O8-Li1-O1-S1	73.1(3)	O5-C3-O6-C4	174.35(17)
O11-Li1-O1-S1	-173.4(2)	O7-C3-O6-C4	-5.7(2)
O5-Li1-O1-S1	-46.7(3)	O5-C3-O7-C5	175.27(18)
O1'-Li1-O1-S1	51.7(13)	O6-C3-O7-C5	-4.7(2)
$O4^1$-Li1-O1-S1	-158.9(7)	C3-O6-C4-C5	12.89(19)
O3-S2-$O4-Li1^2$	-83.5(4)	C3-O7-C5-C4	12.3(2)
N1-S2-$O4-Li1^2$	51.8(4)	O6-C4-C5-O7	-14.61(18)
C2-S2-$O4-Li1^2$	161.5(3)	O11-Li1-O8-C6	107.7(3)
O1-S1-N1-S2	-158.06(12)	O5-Li1-O8-C6	-68.4(3)
O2-S1-N1-S2	-20.85(17)	O1-Li1-O8-C6	-165.0(2)
C1-S1-N1-S2	92.58(14)	O1'-Li1-O8-C6	-156.6(6)
O4-S2-N1-S1	-157.57(12)	$O4^1$-Li1-O8-C6	24.7(3)
O3-S2-N1-S1	-21.60(17)	Li1-O8-C6-O9	41.1(3)
C2-S2-N1-S1	92.44(13)	Li1-O8-C6-O10	-140.6(2)
O1-S1-C1-F1	61.8(2)	O8-C6-O9-C7	-178.4(2)
O2-S1-C1-F1	-62.9(2)	O10-C6-O9-C7	3.1(2)
N1-S1-C1-F1	175.5(2)	O8-C6-O10-C8	-178.21(19)
O1-S1-C1-F2	-177.5(2)	O9-C6-O10-C8	0.3(2)
O2-S1-C1-F2	57.8(2)	C6-O9-C7-C8	-4.9(2)
N1-S1-C1-F2	-63.8(2)	C6-O10-C8-C7	-3.3(2)
O1-S1-C1-F3	-59.3(2)	O9-C7-C8-O10	4.8(2)
O2-S1-C1-F3	176.0(2)	O8-Li1-O11-C9	-76.3(5)
N1-S1-C1-F3	54.4(2)	O5-Li1-O11-C9	99.4(5)

O4-S2-C2-F5	-178.60(14)	O1-Li1-O11-C9	-172.7(4)
O3-S2-C2-F5	57.25(16)	O1'-Li1-O11-C9	-156.3(7)
N1-S2-C2-F5	-65.21(15)	O4[1]-Li1-O11-C9	10.3(4)
O4-S2-C2-F4	-56.69(16)	Li1-O11-C9-O12	92.5(4)
O3-S2-C2-F4	179.15(14)	Li1-O11-C9-O13	-104.9(5)
N1-S2-C2-F4	56.70(16)	O11-C9-O12-C10'	165.5(3)
O4-S2-C2-F6	61.36(14)	O13-C9-O12-C10'	1.8(3)
O3-S2-C2-F6	-62.80(14)	O11-C9-O13-C11	-167.4(3)
N1-S2-C2-F6	174.75(12)	O12-C9-O13-C11	-2.9(4)
O8-Li1-O5-C3	68.5(4)	C9-O12-C10'-C11	0.2(4)
O11-Li1-O5-C3	-107.0(3)	O12-C10'-C11-O13	-1.9(5)
O1-Li1-O5-C3	168.9(3)	C9-O13-C11-C10'	2.9(5)
O1'-Li1-O5-C3	145.9(8)		

1. -x+1/2, y, z+1/2
2. -x+1/2, y,-1+ z+1/2

$(EC)_1$:LiTFSI:

Data Collection and Processing. The sample was mounted on a glass capillary with a small amount of Paratone N oil. All X-ray measurements were made on a Bruker-Nonius Kappa Axis X8 Apex2 diffractometer at a temperature of 110 K. The unit cell dimensions were determined from a symmetry constrained fit of 9829 reflections with $5.8° < 2\theta < 68.94°$. The data collection strategy was a number of ω and φ scans which collected data up to 75.76° (2θ). The frame integration was performed using SAINT.[9] The resulting raw data was scaled and absorption corrected using a multi-scan averaging of symmetry equivalent data using SADABS.[9]

Structure Solution and Refinement. The structure was solved by direct methods using the XS program.[11] All non-hydrogen atoms were obtained from the initial solution. The hydrogen atoms were introduced at idealized positions and were allowed to refine isotropically. The structural model was fit to the data using full matrix least-squares based on F^2. The calculated structure factors included corrections for anomalous dispersion from the usual tabulation. The structure was refined using the XL program from SHELXTL,[11] graphic plots were produced using the NRCVAX crystallographic program suite.[12]

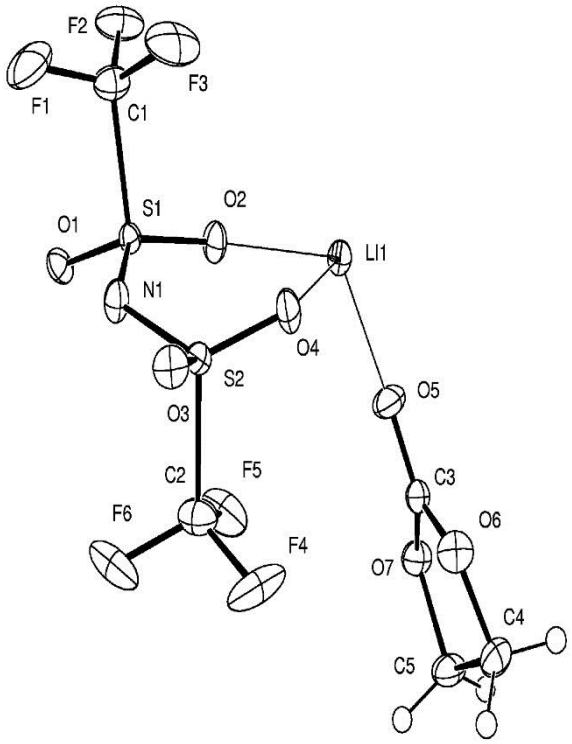

Figure S18. ORTEP drawing of $(EC)_1$:LiTFSI asymmetric unit showing naming and numbering scheme. Ellipsoids are at the 50% probability level and hydrogen atoms were drawn with arbitrary radii for clarity.

Table S8. Summary of crystal data for $(EC)_1$:LiTFSI

formula	$C_5H_4F_6LiNO_7S_2$
formula weight (g mol^{-1})	375.15
crystal dimensions (mm)	0.44 × 0.33 × 0.31
crystal color and habit	colourless prism
crystal system	orthorhombic
space group	$P2_12_12_1$
temperature (K)	110
a (Å)	5.79510(10)
b (Å)	12.7103(2)
c (Å)	16.8547(3)
α (°)	90.00
β (°)	90.00
γ (°)	90.00
V ($Å^3$)	1241.47(4)
number of reflections to determine final unit cell	9829
min and max 2θ for cell determination (°)	5.80, 68.94
Z	4
F(000)	744
ρ (g cm^{-3})	2.007
λ (Å) (MoKα)	0.71073
μ (cm^{-1})	0.542
diffractometer type	Bruker-Nonius Kappa Axis X8 Apex2
scan type (s)	omega and phi scans
max 2θ for data collection (°)	75.76
measured fraction of data	0.990
number of reflections measured	51077
unique reflections measured	5986
R_{merge}	0.0289
number of reflections included in refinement	5986
cut off threshold expression	>2sigma(I)
structure refined using	full matrix least-squares using F^2
weighting scheme	calc w=1/[$sigma^2(Fo^2)$+(0.0411P)^2+ 0.2258P] where P=(Fo^2+2Fc^2)/3
number of parameters in least-squares	216
R_1	0.0332
wR_2	0.0743
R_1 (all data)	0.0395
wR_2 (all data)	0.07709
GOF	1.065
maximum shift/error	0.001
min & max peak heights on final ΔF Map (e^- $Å^{-1}$)	-0. 268, 0. 589

$R_1 = \Sigma(|F_o| - |F_c|)/\Sigma F_o$

$wR_2 = [\Sigma(w(F_o^2 - F_c^2)^2)/\Sigma(w F_o^4)]^{1/2}$

$GOF = [\Sigma(w(F_o^2 - F_c^2)^2)/(\text{No. of reflns. - No. of params.})]^{1/2}$

Table S9. Atomic Coordinates for $(EC)_1$:LiTFSI

Atom	x	y	z	$U_{iso/equiv}$
Li1	-0.1275(4)	0.28963(19)	0.72561(13)	0.0189(4)
S1	0.36985(5)	0.33047(2)	0.806999(16)	0.01245(5)
S2	0.15777(5)	0.51340(2)	0.754017(17)	0.01324(5)
O1	0.60366(15)	0.29465(7)	0.79923(6)	0.01790(16)
O2	0.19497(17)	0.27059(7)	0.76668(6)	0.01897(18)
O3	0.15156(18)	0.61854(6)	0.78400(6)	0.01927(17)
O4	-0.05592(16)	0.45702(7)	0.74707(6)	0.02026(18)
N1	0.35914(19)	0.45299(8)	0.79730(7)	0.01792(19)
C1	0.3050(3)	0.31461(11)	0.91275(8)	0.0225(3)
F1	0.4592(2)	0.36558(10)	0.95586(6)	0.0465(3)
F2	0.3082(2)	0.21455(8)	0.93284(6)	0.0347(2)
F3	0.0975(2)	0.35306(10)	0.92792(7)	0.0438(3)
C2	0.2699(3)	0.52522(11)	0.65264(8)	0.0252(3)
F4	0.1347(3)	0.58827(10)	0.61160(6)	0.0515(3)
F5	0.2735(2)	0.43105(8)	0.61844(6)	0.0366(3)
F6	0.4808(2)	0.56411(8)	0.65342(7)	0.0372(3)
O5	-0.1532(2)	0.29821(9)	0.61210(6)	0.0299(2)
O6	-0.2765(2)	0.42239(8)	0.52762(6)	0.0236(2)
O7	-0.09974(18)	0.28093(8)	0.48206(6)	0.02125(19)
C3	-0.1757(2)	0.33193(10)	0.54582(7)	0.0176(2)
C4	-0.3059(3)	0.42653(11)	0.44192(9)	0.0243(3)
C5	-0.1347(3)	0.34680(11)	0.41257(8)	0.0248(3)
H4A	-0.271(4)	0.4995(15)	0.4253(11)	0.027(5)
H4B	-0.462(4)	0.4064(15)	0.4313(12)	0.023(5)
H5A	-0.192(4)	0.2971(17)	0.3676(13)	0.039(6)
H5B	0.012(3)	0.3743(13)	0.3978(11)	0.017(4)

Table S10. Anisotropic Displacement Parameters for $(EC)_1$:LiTFSI

Atom	u^{11}	u^{22}	u^{33}	u^{12}	u^{13}	u^{23}
Li1	0.0148(10)	0.0252(10)	0.0167(9)	-0.0012(9)	-0.0018(8)	0.0002(8)
S1	0.01129(10)	0.01191(9)	0.01415(11)	0.00026(9)	-0.00012(9)	0.00016(8)
S2	0.01296(11)	0.01254(10)	0.01423(11)	0.00091(8)	0.00063(9)	0.00074(9)
O1	0.0127(4)	0.0181(4)	0.0229(4)	0.0021(3)	0.0033(3)	0.0023(3)
O2	0.0181(4)	0.0142(3)	0.0246(4)	-0.0028(3)	-0.0055(3)	-0.0018(3)
O3	0.0236(4)	0.0129(3)	0.0212(4)	0.0029(3)	0.0012(4)	-0.0012(3)
O4	0.0122(3)	0.0205(4)	0.0281(5)	-0.0009(3)	-0.0020(4)	0.0012(4)
N1	0.0162(4)	0.0126(4)	0.0250(5)	0.0002(3)	-0.0060(4)	0.0010(3)
C1	0.0269(6)	0.0228(6)	0.0177(5)	0.0059(5)	0.0051(5)	0.0017(4)
F1	0.0655(9)	0.0571(7)	0.0170(4)	-0.0132(6)	-0.0083(5)	-0.0042(5)
F2	0.0490(6)	0.0275(4)	0.0277(4)	0.0093(4)	0.0137(4)	0.0130(4)
F3	0.0421(6)	0.0513(6)	0.0379(6)	0.0260(5)	0.0239(5)	0.0120(5)
C2	0.0352(7)	0.0221(6)	0.0182(5)	-0.0036(6)	0.0056(5)	-0.0008(5)
F4	0.0759(9)	0.0570(7)	0.0215(4)	0.0149(7)	-0.0050(6)	0.0157(5)
F5	0.0494(6)	0.0316(5)	0.0289(5)	-0.0147(5)	0.0174(4)	-0.0152(4)
F6	0.0429(6)	0.0277(5)	0.0411(6)	-0.0152(4)	0.0243(5)	-0.0069(4)
O5	0.0359(6)	0.0376(6)	0.0161(4)	-0.0149(5)	-0.0075(4)	0.0072(4)
O6	0.0297(5)	0.0190(4)	0.0223(5)	0.0031(4)	0.0034(4)	-0.0033(4)

O7	0.0217(5)	0.0205(4)	0.0216(4)	0.0054(3)	0.0028(4)	0.0029(3)
C3	0.0164(5)	0.0205(5)	0.0160(5)	-0.0051(4)	-0.0022(4)	0.0007(4)
C4	0.0255(7)	0.0230(6)	0.0245(6)	0.0031(5)	-0.0039(5)	0.0062(5)
C5	0.0293(7)	0.0297(6)	0.0155(5)	0.0025(6)	0.0036(5)	0.0033(5)

Table S11. Bond Lengths for $(EC)_1$:LiTFSI

Li1-O5	1.922(2)	C1-F1	1.3211(19)
Li1-O1[1]	1.993(3)	C1-F3	1.3231(17)
Li1-O2	2.007(3)	C2-F6	1.3185(19)
Li1-O3[2]	2.185(3)	C2-F4	1.3169(19)
Li1-O4	2.198(3)	C2-F5	1.3288(17)
S1-O1	1.4354(9)	O5-C3	1.2036(15)
S1-O2	1.4381(10)	O6-C3	1.3257(16)
S1-N1	1.5671(10)	O6-C4	1.4554(18)
S1-C1	1.8327(14)	O7-C3	1.3299(16)
S2-O3	1.4291(9)	O7-C5	1.4539(16)
S2-O4	1.4356(9)	C4-C5	1.502(2)
S2-N1	1.5759(11)	C4-H4A	0.99(2)
S2-C2	1.8342(14)	C4-H4B	0.96(2)
O1-Li1[3]	1.993(3)	C5-H5A	1.04(2)
O3-Li1[4]	2.185(3)	C5-H5B	0.950(19)
C1-F2	1.3162(16)		

1. -1+x, y, z
2. -x,-1/2+y, 3/2-z
3. 1+x, y, z
4. -x, 1/2+y, 3/2-z

Table S12. Bond Angles for $(EC)_1$:LiTFSI

O5-Li1-O1[1]	123.86(14)	F1-C1-F3	109.09(13)
O5-Li1-O2	114.99(13)	F2-C1-S1	110.71(9)
O1[1]-Li1-O[2]	121.13(12)	F1-C1-S1	110.02(10)
O5-Li1-O3[2]	88.72(10)	F3-C1-S1	109.49(10)
O1[1]-Li1-O3[2]	91.61(10)	F6-C2-F4	109.18(13)
O2-Li1-O3[2]	88.00(10)	F6-C2-F5	109.13(13)
O5-Li1-O4	97.10(11)	F4-C2-F5	109.24(13)
O1[1]-Li1-O4	90.80(10)	F6-C2-S2	110.48(11)
O2-Li1-O4	83.36(9)	F4-C2-S2	109.17(11)
O3[2]-Li1-O4	171.03(13)	F5-C2-S2	109.63(10)
O1-S1-O2	117.02(6)	C3-O5-Li1	162.27(13)
O1-S1-N1	110.06(6)	C3-O6-C4	108.21(10)
O2-S1-N1	116.66(6)	C3-O7-C5	108.91(10)
O1-S1-C1	104.32(6)	O5-C3-O6	124.83(13)
O2-S1-C1	104.89(7)	O5-C3-O7	122.73(13)
N1-S1-C1	101.69(6)	O6-C3-O7	112.44(11)
O3-S2-O4	118.29(6)	O6-C4-C5	103.02(11)
O3-S2-N1	108.10(6)	O6-C4-H4A	106.9(11)
O4-S2-N1	115.67(6)	C5-C4-H4A	113.8(12)
O3-S2-C2	105.17(6)	O6-C4-H4B	106.6(12)
O4-S2-C2	105.70(7)	C5-C4-H4B	112.5(12)

N1-S2-C2	102.05(7)	H4A-C4-H4B	113.1(16)
S1-O1-Li1[3]	143.61(9)	O7-C5-C4	102.44(11)
S1-O2-Li1	139.04(9)	O7-C5-H5A	106.3(12)
S2-O3-Li1[4]	154.96(9)	C4-C5-H5A	116.0(13)
S2-O4-Li1	131.26(9)	O7-C5-H5B	107.4(11)
S1-N1-S2	124.18(7)	C4-C5-H5B	115.3(10)
F2-C1-F1	108.85(13)	H5A-C5-H5B	108.5(17)
F2-C1-F3	108.66(13)		

1. -1+x, y, z
2. -x, -3/2+ y, 3/2-z
3. 1+x, y, z
4. -x, 1/2+y, 3/2-z

Table S13. Torsion Angles for $(EC)_1$:LiTFSI

O2-S1-O1-Li1[1]	76.22(16)	O1-S1-C1-F1	55.39(11)
N1-S1-O1-Li1[1]	-60.04(16)	O2-S1-C1-F1	178.96(10)
C1-S1-O1-Li1[1]	-168.45(15)	N1-S1-C1-F1	-59.09(11)
O1-S1-O2-Li1	-158.26(13)	O1-S1-C1-F3	175.26(10)
N1-S1-O2-Li1	-24.88(16)	O2-S1-C1-F3	-61.16(12)
C1-S1-O2-Li1	86.73(14)	N1-S1-C1-F3	60.79(12)
O5-Li1-O2-S1	107.24(15)	O3-S2-C2-F6	62.15(11)
O1[2]-Li1-O2-S1	-74.43(19)	O4-S2-C2-F6	-171.95(10)
O3[3]-Li1-O2-S1	-165.10(10)	N1-S2-C2-F6	-50.61(11)
O4-Li1-O2-S1	12.48(16)	O3-S2-C2-F4	-57.92(12)
O4-S2-O3-Li1[4]	-91.0(2)	O4-S2-C2-F4	67.97(12)
N1-S2-O3-Li1[4]	135.1(2)	N1-S2-C2-F4	-170.68(11)
C2-S2-O3-Li1[4]	26.7(2)	O3-S2-C2-F5	-177.55(11)
O3-S2-O4-Li1	-167.48(10)	O4-S2-C2-F5	-51.65(13)
N1-S2-O4-Li1	-36.93(13)	N1-S2-C2-F5	69.69(12)
C2-S2-O4-Li1	75.14(12)	O1[2]-Li1-O5-C3	78.9(5)
O5-Li1-O4-S2	-92.95(13)	O2-Li1-O5-C3	-102.8(4)
O1[2]-Li1-O4-S2	142.77(10)	O3[3]-Li1-O5-C3	170.0(4)
O2-Li1-O4-S2	21.51(14)	O4-Li1-O5-C3	-16.9(5)
O3[3]-Li1-O4-S2	37.2(9)	Li1-O5-C3-O6	-22.9(5)
O1-S1-N1-S2	142.76(8)	Li1-O5-C3-O7	157.0(4)
O2-S1-N1-S2	6.33(12)	C4-O6-C3-O5	-170.16(13)
C1-S1-N1-S2	-107.10(10)	C4-O6-C3-O7	9.90(15)
O3-S2-N1-S1	156.09(8)	C5-O7-C3-O5	-174.85(13)
O4-S2-N1-S1	20.83(12)	C5-O7-C3-O6	5.10(15)
C2-S2-N1-S1	-93.35(10)	C3-O6-C4-C5	-19.84(15)
O1-S1-C1-F2	-64.97(12)	C3-O7-C5-C4	-17.02(15)
O2-S1-C1-F2	58.61(12)	O6-C4-C5-O7	21.51(14)
N1-S1-C1-F2	-179.44(11)		

1. 1+x, y, z
2. -1+x, y, z
3. -x, -1/2+y, 3/2-z
4. -x, 1/2+y, 3/2-z

References

1 S. P. Verevkin, A. V. Toktonov, Y. Chernyak, B. Schäffner and A. Börner, *Fluid Phase Equil.*, 2008, **268**, 1.

2 M. J. Frisch, G. W. Trucks, H. B. Schlegel, G. E. Scuseria M. A. Robb, J. R. Cheeseman and G. Scalmani, Gaussian 09, Revision B. 2009.

3 A. V. Marenich, C. J. Cramer and D. G. Truhlar, *J. Phys. Chem. B*, 2009, **113**, 6378.

4 S. Trasatti, *Pure Appl. Chem.*, 1986, **58**, 955.

5 O. Borodin and T. R. Jow, *ECS Trans.*, 2011, **33**, 77.

6 O. Borodin, W. Behl and T. R. Jow, *J. Phys. Chem. C*, 2013, **117**, 8661.

7 L. Xing and O. Borodin, *Phys. Chem. Chem. Phys.*, 2012, **14**, 12838.

8 J. Vatamanu, O. Borodin and G. D. Smith, *J. Phys. Chem. C*, 2012, **116**, 1114.

9 Bruker. SAINT and SADABS. Bruker AXS Inc., 2009, Madison, Wisconsin, USA.

1 A. Altomare, G. Cascarano, C. Giacovazzo, A. Guagliardi, M. C. Burla, G. Polidori and M. J. Camalli, *Appl. Crystallogr.*, 1994, **27**, 435.

11 G. M. Sheldrick, *Acta Crystallogr.*, 2008, **A64**, 112.

12 E. J. Gabe, Y. Le Page, J. P. Charland, F. L. Lee and P. S. White, *J. Appl. Crystallogr.*, 1989, **22**, 384.